^2H NMR STUDIES OF THE EFFECT OF THE DPPC/DPPG RATIO ON BILAYER PROPERTIES IN THE PRESENCE OF Ca^{2+}

MARIA KILFOIL

^{2}H NMR studies of the effect of the DPPC/DPPG ratio on bilayer properties in the presence of Ca^{2+}.

by

©Maria Kilfoil

B.Sc. (University of New Brunswick, Fredericton, New Brunswick, Canada) 1995

A thesis submitted to the School of Graduate

Studies in partial fulfillment of the

requirements for the degree of

Master of Science

Department of Physics and Physical Oceanography

Memorial University of Newfoundland

June, 1997

St. John's Newfoundland

I heard a perfect echo die

into an anonymous wall of digital sound

somewhere deep inside

of my soul

A natural beauty should be

preserved like a monument

Don't judge yourself too harsh my friend

or someday you might find your soul endangered

-Neil Young

Abstract

The presence of Ca^{2+} ions in the aqueous medium is known to influence the physical properties of bilayer membranes containing charged phospholipids such as dipalmitoylphosphatidylglycerol (DPPG). ^2H NMR has been used to study the effect of Ca^{2+} on the order, dynamics and phase behaviour of bilayers containing mixtures of the anionic DPPG and a neutral lipid with identical acyl chains, dipalmitoylphosphatidylcholine (DPPC), dispersed in aqueous solutions. The effect of bilayer surface charge in this system was investigated by varying the DPPG/DPPC ratio in the presence of excess Ca^{2+}. It was found that Ca^{2+} alters the temperature and width of the liquid crystal to gel bilayer transition and the quadrupole echo relaxation times of chain deuterons in a way which depends on the proportion of negatively charged lipid in the bilayer. The observed effects are consistent with a Ca^{2+}-induced reduction in area per lipid of liquid crystal bilayers containing DPPG. The results do not support a preferential association of Ca^{2+} with the DPPG headgroup or segregation into DPPG or DPPC domains. The introduction of a negatively charged lipid component into DPPC membranes may alter the hydrogen bonding or modify the water layer, or both, resulting in changes in the adiabatic bilayer motions.

Table of Contents

List of Tables

List of Figures

1

Introductory Remarks

Nuclear magnetic resonance (NMR) is a spectroscopic technique which, in general, provides information on the molecular level. Deuterium NMR spectral frequencies depend on the orientation of the electric field gradient at the deuterium nucleus. Broadening of spectral lines is due to interactions which depend on molecular orientation and the separation of molecules and are thus influenced by molecular motion. This gives rise to the concept of a spectroscopic timescale. The spectroscopic timescale for ^{2}H NMR, $\tau_s \approx 10^{-6}s$ [1], is long enough that molecular motions often give rise to appreciable motional averaging, and thus NMR occupies a unique place among spectroscopic techniques.

Motions can be divided into two classes. Slow motions which have correlation times τ_c satisfying $\tau_c \gg \tau_s$ have negligible influence on the spectrum. Fast motions, i.e. those for which $\tau_c \ll \tau_s$, give rise to motional averaging in which the rigid lattice spectrum is transformed into one that is an average over fast motions. Local structural information is obtained from the ^{2}H NMR spectrum, whereas information on molecular motions is provided by relaxation time measurements.

This chapter is devoted to membranes, in particular model membranes. Membrane and lipid structure and dynamics are discussed and order of magnitude timescales are

given for the array of motions. Lipid phase transitions are briefly reviewed and some results of studies on binary lipid mixtures in the aqueous environment are discussed.

1.1 The Lipid Bilayer

1.1.1 Lipid Bilayer Structure

Biological membranes are comprised of aggregates of lipids and proteins that are associated with each other without covalent bonds. Lipids such as phospholipids, cholesterol, and glycolipids not only provide a matrix for the proteins (figure 1.1) and stabilise particular regions of the bilayer, but are almost certainly involved in protein function. The

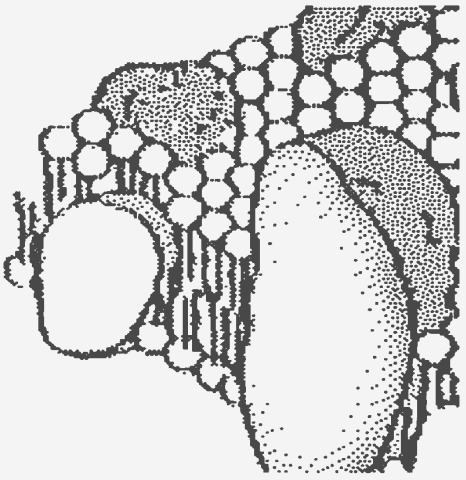

Figure 1.1: Schematic cross-section of a typical biological membrane.

remarkable variety of lipids found in membranes and the ability of organisms to alter membrane composition in response to a perturbing stimulus lend support to this view.

The self-assembly of lipid and protein components into specific macromolecular organisations when hydrated is governed largely by the hydrophobic effect. This is a solvent-induced effect which has been described in detail elsewhere [2] [3]. In short, the

magnitude of the hydrophobic effect is directly related to the exposed surface area of the lipid molecule that is unable to interact with the structure of water; i.e. unable to form hydrogen bonds. Methyl and methylene groups cannot donate or accept hydrogen bonds. For amphipathic molecules which have both hydrophilic and hydrophobic portions, the optimum free energy is achieved with a molecular organisation that maximises the interaction of the polar regions with the water structure and minimises the exposure of the hydrocarbon regions to the aqueous phase. This leads to an area per headgroup at which the free energy is a minimum [4].

A very common type of lipid, the phospholipid, has a hydrophobic region composed of two acyl chains attached via a glycerol backbone to a phosphatidyl headgroup which often, but not always, has a polar character (figure 1.2). The two lipids under study have identical 16-carbon chains but differ in their headgroup structures. They are shown schematically in figure 1.2. Dipalmitoylphosphatidylcholine (DPPC) is zwitterionic with a temporary dipole as opposed to the dipalmitoylphosphatidylglycerol (DPPG) which carries one negative charge at neutral pH. These lipids tend to form membrane-like bilayers wherein the polar headgroups are exposed to the aqueous environment, while the hydrophobic acyl chains extend into the bilayer interior away from the water and are roughly aligned. This lends them the important characteristic of uniaxial symmetry.

The acyl chains in the bilayer interior interact mainly through fairly well-understood van der Waals attractive and steric repulsive forces [5]. The hydrophilic headgroup region contains hydrated and/or ionised groups in contact with the aqueous medium. In addition to steric interactions, the headgroup region experiences dipolar and electrostatic forces

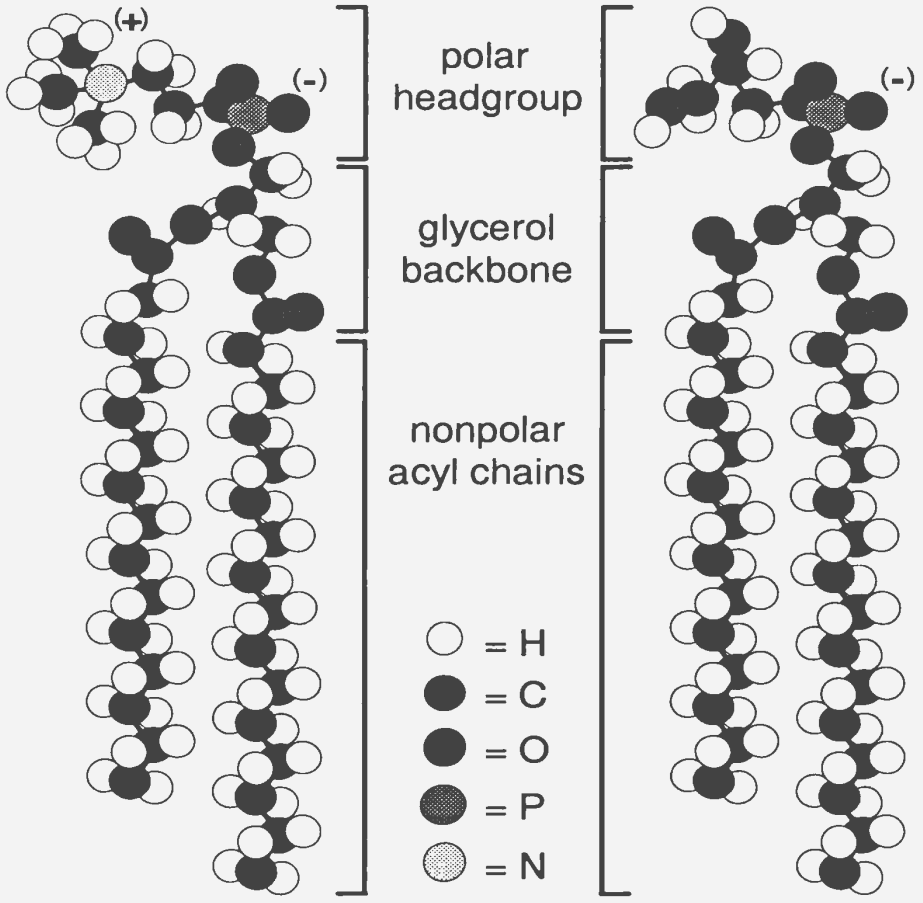

Figure 1.2: Schematic space-filling representation of dipalmitoylphosphatidylcholine (left) and dipalmitoylphosphatidylglycerol (right). DPPC is zwitterionic with a temporary dipole while DPPG carries one negative charge at neutral pH.

involving bound and free counterions, strongly associated water and hydrogen bonds. It has been suggested that headgroup structure should be considered less an intrinsic property of a particular lipid than one that depends on the interactions with neighbouring headgroups [5]. An analogous conclusion should apply to lipid chains.

Protons can be replaced by deuterons at specific locations on lipid molecules by means of chemical synthesis or biochemical incorporation. Virtually all regions of a phospholipid molecule, i.e. the polar headgroup, gycerol backbone or fatty acid chains, are accessible to these techniques. The replacement of a proton with a deuteron is not expected to

perturb the system appreciably and thus preserves, and reports on, the natural structure and dynamics of the membrane. Since the natural abundance of deuterium is low the deuterium NMR signal can immediately be assigned to the deuterium labelled site. Samples in this study contained lipids with perdeuterated chains, which require much less time for both sample preparation and NMR measurements.

1.1.2 Lipid Bilayer Dynamics

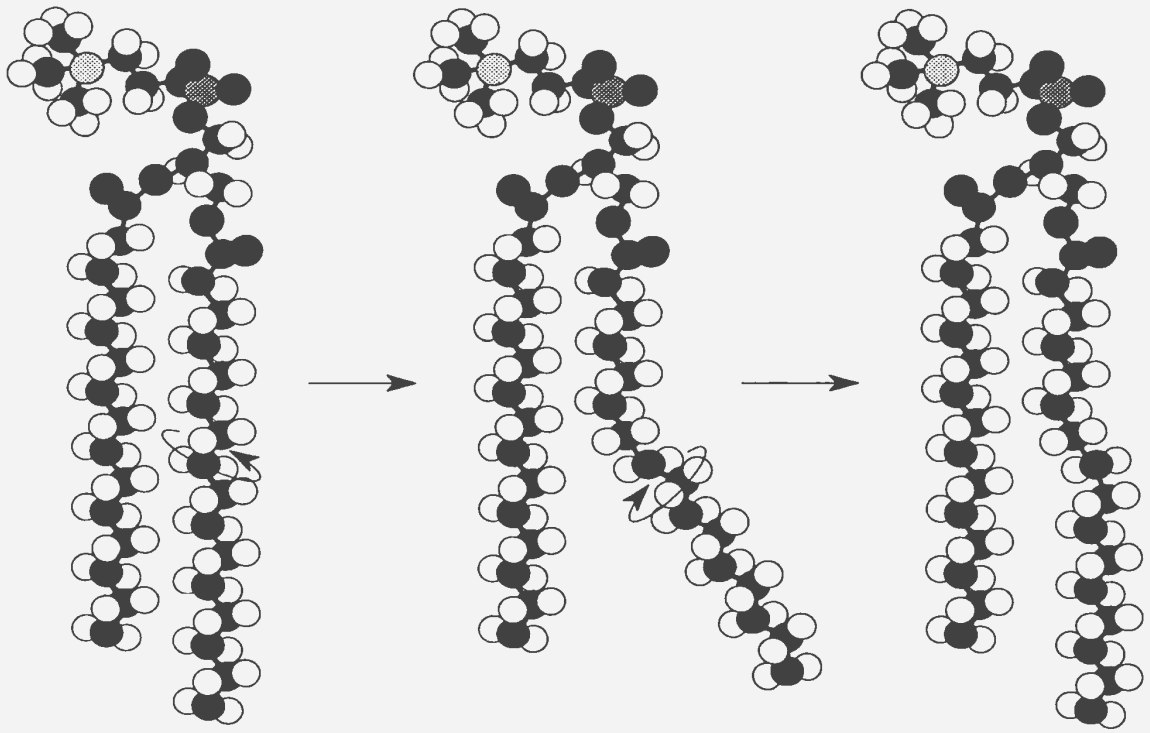

Figure 1.3: Chain isomerisation: trans-gauche isomerisation in dipalmitoylphosphatidylcholine.

A highly dynamic state of the lipid bilayer is necessary for the function of biological membranes, which usually are in a liquid crystalline state. Lipids in bilayers typically undergo a hierarchy of motions on quite different timescales. Measurement of ^{2}H NMR relaxation provides information on the correlation times characterising the relevant motional rates.

At this point, only the order of magnitude of timescales are accessible. A unique and quantitatively consistent picture of phospholipid dynamics has not yet emerged [6]. This is mainly due to the complexity of the system and the fact that, in general, models must be constructed to interpret the measurements of the dynamic properties.

The molecular motions which lead to motional averaging of the quadrupolar interactions are, by definition, short on the NMR timescale (i.e. $\tau_c \leq 10^{-6}s$). Of the motions accessible by NMR, *trans-gauche* isomerisation is the fastest, having a correlation time $\tau_J < 10^{-10}$s [7]. As shown in 1.3, single bond rotations introduce kinks and jogs into a fully-ordered chain while still maintaining a net orientation parallel to the bilayer normal. Another motion on approximately the same timescale is rotational diffusion where the

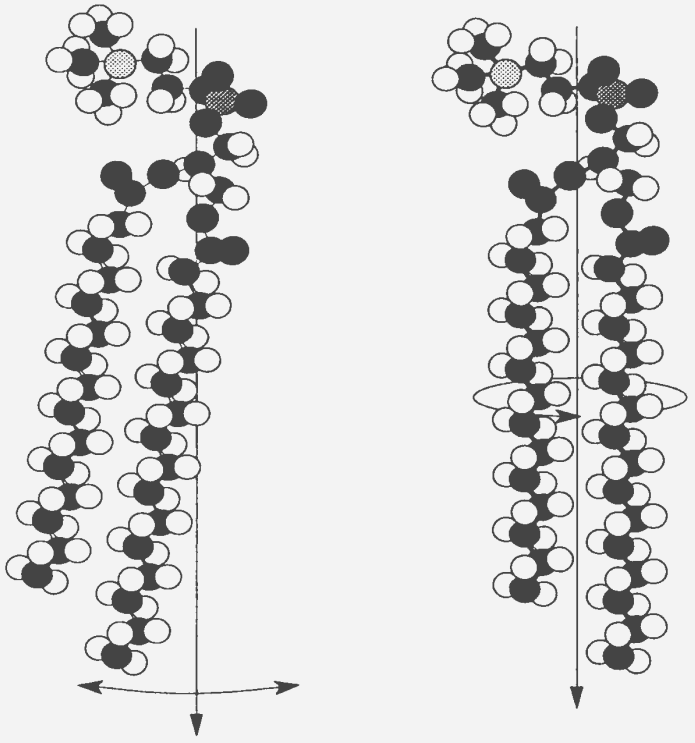

Figure 1.4: Chain reorientation: libration and rotational diffusion in dipalmitoylphosphatidylcholine corresponding to the correlation times discussed in the text for the phospholipid molecule in a bilayer.

individual lipid molecules rotate very rapidly about their long axes. It is characterised by the correlation time $\tau_{||}$, following the notation of Yeagle [8]. These fast motions contribute to transverse relaxation, but slow motions also make important contributions [9] [10].

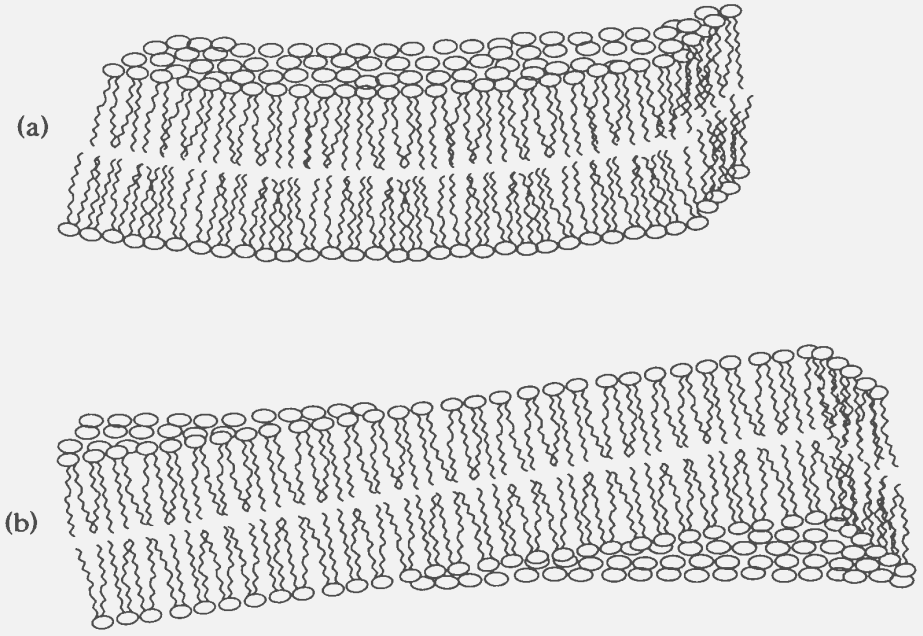

Figure 1.5: Examples of bilayer collective undulation modes: splay mode (a) and twist mode (b).

Of course the definition of slow motions depends on the measurement technique and what the technique is sensitive to. Motions which are slow on the NMR timescale (i.e. adiabatic motions) include lateral diffusion of the phospholipids as well as collective motions and undulations of the bilayer. Bloom *et al.* [1] describe slow motions associated with molecular diffusion on a spherical surface. Lipid molecules readily exchange places with their neighbours within a bilayer ($\approx 10^7$ times per second) and this gives rise to a lateral diffusion constant $D \approx 4 \times 10^{-12} m^2 s^{-1}$ [9] for multilamellar vesicles.

It has recently been argued that collective lipid motions constitute the dominant

transverse relaxation process [10] in lipid bilayers. The time-dependent fluctuation of the orientation of the director for axial diffusion is often called chain libration or wobble. It is convenient to think of this motion as one in which the axis for axial diffusion randomly samples a cone of finite dimension, with extreme angular deflections of individual lipids limited by the presence of neighbouring lipids. Chain tilting is likely to be at least locally cooperative since one phospholipid cannot wobble into space occupied by another phospholipid unless the latter leaves that same space on the same timescale. Director fluctuations are characterised by the correlation time $\tau_\perp = 10^{-8}$ to 10^{-4}s [11]. The collective undulations occur over a very wide timescale ranging from $10^{-6}s$ to $10^{1}s$ [12].

1.1.3 Phase Transitions in Anionic and Mixed Bilayers

The lipid chains possess a tendency to go from a fully ordered gel state to a fluid or liquid crystalline state. The transition between these phases is often called the chain-melting transition and occurs at a characteristic temperature T_m determined by the thermodynamic parameters of the system. It is accompanied by changes in both the angular amplitude of chain motion and the rates of motion. By convention the liquid crystalline state is designated L_α and the condensed gel phase is called L_β.

Bilayers may also undergo transitions to non-lamellar phases in a manner which is particularly sensitive to the local environment. Both thermotropic[1] and lyotropic phase transitions can be induced by varying such factors as lipid concentration, temperature,

[1]The term thermotropic is derived from the Greek roots *thermō*, denoting heat, and *tropikos*, which means of a turn (originally of the sun at the solstices). Hence the term refers to a change in phase induced by heat.

and ionic composition of the aqueous environment. Often DSC, DTA, and NMR measurements are taken at temperature intervals, and so one "follows" the sample through the phase transition.

A fully cooperative transition would manifest itself in an infinitely sharp discontinuity in going from L_α to L_β. The effect of increased surface charge on broadening the chain phase transitions in anionic lipids has been interpreted by Forsythe [13] as a consequence of domain formation: near the transition temperature it is favourable for the system to break up into fluid and gel domains in order to maintain the energy balance referred to in section 1.1.1. Gel and fluid domains will be discussed further in chapter 3 in relation to interpreting ^{2}H NMR spectra exhibiting two-phase coexistence.

The chemical nature and charge of the lipid headgroup can affect the melting point, but not always in a manner based on simple electrostatic considerations. The chain melting transition for pure DPPC-d_{62} and pure DPPG-d_{62} multilamellar vesicles occurs at 37°C. This similarity is striking considering the difference in headgroups between the two species. In contrast, doubly ionised DPPA has a T_m 16°C higher [14], and electrically neutral DMPE melts at 48°, 25° higher than DMPC [15].

When calcium ions are present in the hydrating buffer, pure DPPG exhibits a very complex phase behaviour. This seems to indicate a great flexibility in the interactions of the phosphoglycerol headgroup at the bilayer surface. In aqueous systems containing calcium the transition temperature of pure DPPG-d_{62} occurs at 86°C [16] while that for pure DPPC-d_{62} remains largely unchanged. This is an extreme temperature for the experimental apparatus used in this study, making examination of compositions above

80% DPPG impractical.

1.1.4 Anionic and Mixed Bilayers in the Aqueous Environment

Bilayer hydration depends mainly on the type and state of the headgroup. Hydration of the chains is a much smaller effect and exists mainly as interactions between water and the carbonyl groups on the acyl chains. While acyl chain and headgroup interactions are often discussed separately, they are of course interdependent. Ions in the aqueous phase can alter the stereochemistry of the headgroup region and influence the packing requirements of the lipid molecule. Similarly the degree of hydration of the interfacial region and the depth of water penetration into the bilayer can influence the conformational freedom of the lipid acyl chains.

Numerous attempts such as those by Marčelja [4] and Finer and Darke [17] have been made to model the electrostatic interactions of polar headgroups with ions, water molecules and with each other. Marsh and Cevc maintain that coulombic forces play a rather minor role in bilayer hydration [18]. What we refer to as hydration forces are a subgroup of solvent-induced forces (SIF's) and are poorly understood. Their subtle origin lies in the response of the system to perturbations imposed by the presence of solutes on the structure and dynamics of the solvent. This response acts to drive the system towards the attainment of mutual distances and orientations of solutes which minimise the total free energy of the system. The free energy involves opposing contributions from the interaction energy per lipid and the conformational entropy of the chains. Electrostatic forces act through the solvent and with the contribution of the solvent, but the water

affects their size only, not their existence. This is at variance with SIF's, whose very existence for a given configuration of solutes has its origin in the presence and structure of the solvent. While much is known *statistically* about these forces, time and space resolutions down to single molecular events are being sought [2].

The degree of hydration and the nature of hydrogen bonding interactions in the headgroup and interfacial regions of PG bilayers differ significantly from what is observed in all other phospholipid bilayers studied by McElhaney *et al.* [19]. In their recent FTIR and ^{31}P NMR study of pure anionic PG phase behaviour it is proposed that the glycerol backbone of the phosphatidylglycerol headgroup helps shield the negative charges at the surface of the bilayer by means of hydration-like hydrogen bonding interactions with the phosphate on the headgroup. It is suggested that the exposed hydroxyl groups on the glycerol headgroup enable the lipid to mimic some of the solvation properties of water and compete with water molecules for hydration sites. This may confer to phosphoglycerols an important structural role in addition to the negative charge they impart to the bilayer surface.

1.1.5 Previous Results

The important previous experimental results may be summarised as follows. A number of calorimetric [20] [21] [14] and light scattering [20] studies have been concerned with the miscibility of binary phospholipid systems. A DSC study by Jacobson and Papahadjopoulos [14] has shown that in phosphatidylcholine bilayers containing either of the anionic lipids phosphatidylserine (PS) or phosphatidic acid (PA) with exactly similar

chains, addition of Ca^{2+} induces a lateral phase separation. The absence of such behaviour in aqueous mixtures of PG and PC lipids with exactly similar chains indicates a high degree of mixing of the two lipids.

While investigators have emphasised the ability of Ca^{2+} to segregate acidic and neutral lipids [14] [22], PG/PC mixed bilayers with exactly similar chains appear to behave differently. Findlay and Barton [20] could observe Ca^{2+}-induced phase separation in the bilayer by variation of the fatty acid composition of mixed phosphatidylglycerol/phosphatidylcholine bilayers [20]. However, they could not detect a Ca^{2+}-induced phase separation for DPPG/DPPC mixtures. van Dijck et al. [21] found that Ca^{2+} only shifts the transition peak to higher temperatures but no phase separation occurs for up to 80% DPPG composition. That phase separation did not occur was evident in the single thermal transition which progressively increased with increasing proportion of the PG component. At these compositions none of the complex behaviour characteristic of pure DPPG regions [16] was observed. This suggests that the behaviour of acidic/neutral lipid systems in the presence of Ca^{2+} is much more complicated than can be explained on the basis of simple electrostatic considerations.

In a recent Fourier transform infrared (FTIR) study of the thermotropic behaviour of phospholipid bilayers interacting with metal ions [23], Kwon *et al.* argue on the basis of CH_2 stretching modes that DPPG exists in a more disordered state than DPPC in vesicles in the L_α phase. With the addition of Ca^{2+} to the aqueous phase, the DPPG acyl chains change to a more highly-ordered form by Ca^{2+}-induced isothermal crystallization. Their results also suggest that the carbonyl groups in the interfacial region of hydrated

phospholipids take part in hydrogen bonding and are dehydrated by metal ions. The dehydration ability of metal ions should also be a contributing factor to shifting the phase transition temperature.

1.2 Motivation and Thesis Outline

1.2.1 Motivation

Lipid bilayers are fascinating to physicists and chemists because they represent a mechanism of self-assembly into partially ordered systems. The phase transitions of these systems are also of interest because they are usually highly cooperative first-order transitions. In addition to the purely academic interest in such macromolecular organisation, these bilayers play crucial biological roles. Part of the initial motivation for this work was the interesting behaviour of lung surfactant. Lung surfactant is comprised of the proteins SP-B and SP-C, calcium ion and phosphatidylcholine containing a large amount of anionic lipid. In recent studies by Morrow *et al.*, mixed DPPG/DPPC bilayers containing SP-B showed evidence for the formation of freely reorienting bilayer fragments or discs [24], while SP-C displayed a tendency towards non-random lateral distribution in the mixed bilayers [25].

The ability of phospholipids to segregate into domains is of considerable interest in light of the recent evidence that the functions of some membrane-associated enzymes appear to require the presence of anionic lipids for their function [26] [27] [28]. Ca^{2+}-induced phase separations may play an important role in modulating enzyme activity. It seems clear that aside from their role in regulating bilayer surface charge density, anionic

lipids must have more specific functions in biological membranes. These functions are poorly understood at present, and much more work needs to be done before the general and specific roles of anionic lipids in biological membranes are fully understood.

Most of the information about lipid bilayers has come from model membrane systems. They can be prepared from a small number of well-defined components, allowing for a better characterisation of the underlying physical principles which should complement the interpretation of more complex systems. ^{2}H NMR studies of mixed lipid bilayers that contain trans-membrane proteins, for example, must be interpreted with caution. Straightforward conclusions may be complicated and masked by the effects caused by different phospholipid types interacting with each other. The goal of this thesis is to characterise the role of the anionic lipid in the structure and dynamics of binary DPPG/DPPC mixtures under varying ionic conditions, and for a range of temperatures including the physiological.

1.2.2 Thesis Outline

The degree of perturbation of the phospholipid acyl side chains under varying physiological conditions is investigated in order to relate physical properties to biological function. Specific questions addressed in the present work include:

1. *The extent to which the interaction of DPPC/DPPG mixed bilayers is selective.* From purely electrostatic considerations we should expect that effects of the divalent cation would be more prominent for negatively-charged DPPG than for neutral DPPC.

In addition however, a Ca^{2+}-induced change in headgroup orientation of the anionic lipid and expulsion of some of the surrounding water molecules in its hydration layer could introduce steric constraints on both headgroups and side chains of neighbouring lipids via a reduced area per lipid. This would be consistent with previously published results by Sixl *et al.* and Zidovetski *et al.* in which increased ordering is observed upon addition of Ca^{2+} to binary mixtures of DPPG and DPPC deuterated in the headgroup [29] and in the acyl chains [30], respectively. Information concerning molecular conformation and orientational order is obtained from lineshape analysis, providing clues to how lipids pack within the common bilayer.

2. *How the thermotropic behaviour is affected by such induced changes in the surface charge density, both in the presence and absence of calcium.* Regulation of the ionic component in this binary system allows the experimenter to manipulate the surface charge density of the model membrane. The thermotropic behaviour was studied by following the order-disorder transition for each of the samples.

3. *The extent to which bilayer slow motions are sensitive to changes in bilayer surface charge.* Collective order fluctuations usually occur at extremely low frequencies (kHz range) while molecular reorientation and rotational diffusion invariably take place on the MHz scale. These fast and slow motions are probed via relaxation measurements. Again the question arises as to whether the DPPC and DPPG are reporting on the same slow motions in the mixture, and to what extent the motional rates depend on the sample preparation.

The general outline of the thesis is as follows. Experimental techniques are presented below. In chapter 2 the fundamental theory behind deuterium NMR spectroscopy is reviewed. The Hamiltonian for the system is discussed, as are the resulting quadrupolar splittings in the absence and presence of motions which are fast on the NMR timescale. The phenomenon of relaxation is introduced and the timescales for transverse relaxation are discussed. Consideration is given to the quadrupolar echo and techniques for extracting structural and dynamic properties. Appendix A is associated with chapter 2 and provides a detailed picture of the evolution of the spin system during and following a pulse sequence. In appendix B useful information for the general theory calculation is provided. Chapters 3 and 4 contain the experimental results and discussion. Experimental results concerning ordering of the systems under study are presented and discussed in chapter 3. Chapter 4 deals with further results of our investigations as they pertain to lipid dynamics. A discussion of typical rates for the motions under consideration will be followed by experimental results for this study. In chapter 5 concluding remarks are advanced.

1.3 Apparatus

The ^{2}H NMR experiments were performed on a spectrometer constructed by Michael Morrow based on the design of Davis *et al.* [31], and using a superconducting magnet with a field strength of 3.55 Tesla, corresponding to a Larmor frequency of $\omega_0/2\pi = 23.215$ MHz. Spectra were acquired using the quadrupolar echo pulse sequence described in section 2.4. The deuterium probe and the pulse programmer controlling the experiments

were also locally-constructed. Upon instruction by the computer the rf transmitter produces the short $\pi/2$ pulses which are channelled to the probe tank circuit. The probe resonantly excites the nuclei. Once the transmitter pulse has been removed the nuclear signal is free to pass to a low noise preamplifier and high gain receiver. The voltage generated by the receiver is then digitised and sent to the computer to be stored as the time domain signal. Quadrature detection and phase cycling were used to minimise errors due to instrumental imperfections [32]. The spectroscopic bandwidth was 250 kHz for liquid crystalline lipids and 500 kHz for gel phase lipids. Typical $\pi/2$ pulse width was 3.6 μs. The number of scans varied between 4000 and 70 000 depending on the particular sample. Data were collected on a 386 PC and transferred to a Digital Equipment Corporation Alpha workstation for analysis.

A temperature controller was used to maintain constant temperature around the sample using thermocouples placed in the bore of the magnet. Cold nitrogen gas from the evaporation of liquid N_2 was blown over the sample where cooling below room temperature was desired. The accessible range was between 70°C and -20°C.

1.4 Methods and Materials

A number of model membrane systems were used. In each case, the amount of calcium was kept constant and in excess to the presumed stoichiometry of one Ca^{2+} to every two anionic lipids. The buffer was maintained at 10 mM Ca^{2+} and the volume of buffer used was varied depending on the total lipid weight. The negatively-charged lipid component never exceeded 50%. Chain perdeuterated DPPC-d_{62} was synthesised using the acylation

reaction of Gupta et al. [Proc. Natl. Acad. Sci. USA **74**, 4315 (1977)]. Synthetic chain perdeuterated DPPG-d_{62} was purchased from Sigma (St. Louis, MO). Samples were prepared by dissolving each of the lipids in a 3:1 mixture of chloroform and redistilled ethanol before mixing in a flask. The solvents were removed using a rotary evaporator, and residual traces were removed under high vacuum overnight. Multilamellar vesicles (MLV's) were formed by hydrating the mixed lipid with a buffer containing either no calcium (150 mM NaCl, 130 mM HEPES) or the desired concentration of calcium (150 mM NaCl, 130 mM HEPES, 10 mM $CaCl_2$). In this study two hydration protocols were adopted. One involved scraping the dried lipids from the walls of the flask and adding the buffer with gentle stirring. The other involved hydrating the lipids in the flask which was rotated in a hot water bath kept above T_m. The former method was used in all samples unless stated otherwise. The buffer was at pH 7, well above the pK_a of DPPG for maximum ionization of the DPPG. The samples were centrifuged to obtain a pellet which was then transferred to a sample tube for NMR studies. All lipid mixtures contained less than 10% lipid by weight with respect to water.

2

^{2}H NMR Theory

This chapter treats the fundamental theory behind deuterium NMR spectroscopy. The theory underlying the splitting of the Zeeman energy levels by the quadrupolar interaction is first developed in the absence of molecular motions. The expression for the quadrupolar splitting is then expanded to account for motions which modulate the spectrum. The phenomenon of relaxation is introduced and relaxation theory for spin 1 is given here. A discussion of the density matrix will be limited to its utility in treatment of spin $\mathbf{I} = 1$ systems. The quadrupolar echo and techniques for extracting structural and dynamic properties are briefly reviewed. Examples using density matrix and density operator formalism to follow the evolution of a spin system are provided in appendix A.

2.1 ^{2}H Quadrupolar Hamiltonian

The two main contributions to the energy of a deuterium nucleus in a static magnetic field are the Zeeman energy and the quadrupole energy. The Hamiltonian may be written as

$$\mathcal{H} = \mathcal{H}_Z + \mathcal{H}_Q \tag{2.1}$$

where $\mathcal{H}_Z$ is the Zeeman Hamiltonian and $\mathcal{H}_Q$ is the quadrupolar Hamiltonian. $\mathcal{H}_Z$ describes the interaction of the nuclear magnetic moment $\vec{\mu_n}$ with the magnetic field $\vec{B}$.

$$\mathcal{H}_Z = -\vec{\mu_n} \cdot \vec{B} = -\gamma\hbar\vec{I} \cdot \vec{B}$$

where γ is the gyromagnetic ratio of the nucleus in question and $\vec{I}$ is the nuclear spin operator. Taking the field to be B_0 along the z-direction, the Zeeman Hamiltonian is

$$\mathcal{H}_Z = -\gamma\hbar B_0 I_z$$

and the Larmor frequency ω_0 is given by

$$\omega_0 = 2\pi\nu_0 = \gamma B_0.$$

The quadrupolar Hamiltonian $\mathcal{H}_Q$ arises from an electrostatic interaction of the nuclear quadrupole moment $\mathcal{Q}$ with the electric field gradient at the position of the nucleus, $\nabla\vec{E} = V_{jk}$. V_{jk} is a symmetric second rank tensor:

$$V_{jk} = \left.\frac{\partial^2 V}{\partial x_j \, \partial x_k}\right|_{\vec{r}=0} = \begin{pmatrix} V_{11} & V_{12} & V_{13} \\ V_{12} & V_{22} & V_{23} \\ V_{13} & V_{23} & V_{33} \end{pmatrix}.$$

It is convenient to define $\mathcal{H}_Q$ in the lab frame. $\mathcal{Q}$ like any operator can be recast in terms of irreducible tensor operators. For $\mathbf{I} = 1$ only tensors of rank $n \leq 2$ are required by virtue of the Wigner-Eckart theorem [33] and in the case of quadrupolar interaction only the second rank irreducible tensor survives [34], so that $\mathcal{H}_Q$ can be written

$$\mathcal{H}_Q = C_Q \sum_{m=-2}^{+2} (-1)^m T_m^{(2)} V_{-m}^{(2)}. \tag{2.2}$$

The five components of $\mathbf{T}^{(2)}$ in terms of the spin operators I_z and $I_\pm = I_x \pm iI_y$ are

$$\begin{aligned} T_0^{(2)} &= \frac{1}{\sqrt{6}}\left(3I_z^2 - I(I+1)\right) \\ T_{\pm 1}^{(2)} &= \mp\frac{1}{2}\left(I_z I_\pm + I_\pm I_z\right) \\ T_{\pm 2}^{(2)} &= \frac{1}{2} I_\pm I_\pm . \end{aligned}$$

Examination of the matrix elements $\mathcal{Q}_{jk}$ [35] provides

$$C_Q = \frac{eQ}{2I(2I-1)}$$

where eQ is the electric quadrupole moment of the nucleus. The deuterium nucleus spin operators I_x, I_y, I_z are given by

$$I_x = \frac{1}{\sqrt{2}}\begin{pmatrix} 0 & 1 & 0 \\ 1 & 0 & 1 \\ 0 & 1 & 0 \end{pmatrix}, \quad I_y = \frac{i}{\sqrt{2}}\begin{pmatrix} 0 & -1 & 0 \\ 1 & 0 & -1 \\ 0 & 1 & 0 \end{pmatrix}, \quad I_z = \begin{pmatrix} 1 & 0 & 0 \\ 0 & 0 & 0 \\ 0 & 0 & -1 \end{pmatrix}.$$

Because these operators are defined with respect to the magnetic field fixed in the laboratory, $\mathbf{T}^{(2)}$ is defined in the laboratory coordinate system.

The electric field gradient tensor is usually known in a coordinate system defined along the axis of the C-D bond vector. A transformation can be carried out to the coordinate system in which the EFG tensor is diagonalised. In this principal axis system (PAS) of the potential $V_{xx} + V_{yy} + V_{zz} = 0$ where V_{xx}, V_{yy} and V_{zz} are electric field gradients along the three cartesian axes. The asymmetry parameter is defined as

$$\eta = \frac{V_{xx} - V_{yy}}{V_{zz}}.$$

By convention the axes are chosen such that $V_{zz} \geq V_{xx} \geq V_{yy}$ and $0 \leq \eta \leq 1$. The quadrupole Hamiltonian in this system is

$$\mathcal{H}_Q = \frac{eQ}{4I(2I-1)}\left(V_{zz}(3I_z^2 - I^2) + (V_{xx} - V_{yy})(I_x^2 + I_y^2)\right). \tag{2.3}$$

To express the electric field gradient tensor in the laboratory coordinate system it is necessary to transform from the molecular-based reference frame. The EFG is first expressed in a spherical basis set in terms of its irreducible components $V_m^{(2)}$, $m = 0, \pm 1, \pm 2$

$$\begin{aligned} \left(V_0^{(2)}\right)_{PAS} &= V_{zz} = eq \\ \left(V_{\pm 1}^{(2)}\right)_{PAS} &= 0 \\ \left(V_{\pm 2}^{(2)}\right)_{PAS} &= \sqrt{\frac{1}{6}}(V_{xx} - V_{yy}). \end{aligned} \tag{2.4}$$

The transformation from one frame to another involves successive rotations through Euler angles ϕ, θ, ζ (see figure B.1) using the Wigner rotation matrices $D_{mm'}^{(2)}(\phi, \theta, \zeta)$ [34] as defined in appendix B. This gives

$$V_{m'}^{(2)} = \sum_{m=-2}^{2} D_{mm'}^{(2)}(\phi, \theta, \zeta) V_m^{(2)} \tag{2.5}$$

where $D_{mm'}^{(2)}(\phi, \theta, \zeta)$ is expressed in terms of the reduced rotation matrix,

$$D_{mm'}^{(2)}(\phi, \theta, \zeta) = e^{-i\phi m} d_{mm'}^{(2)}(\theta) e^{-i\zeta m'}. \tag{2.6}$$

To first order all but $T_0^{(2)}$ of the components of $\mathbf{T}^{(2)}$ can be neglected [36]. Equation 2.2 becomes

$$\mathcal{H}_Q = C_Q T_0^{(2)} V_0^{(2)}$$

where

$$\begin{aligned} V_0^{(2)} &= \sum_{m=-2}^{+2} D_{m0}^{(2)}(\phi,\theta,\zeta)\left(V_m^{(2)}\right)_{PAS} \\ &= \frac{1}{2}\left(3\cos^2\theta - 1\right) + \frac{1}{2}\eta eq \sin^2\theta\cos 2\phi \end{aligned}$$

using equations 2.4 - 2.6 and

$$d_{-20}^{(2)} = d_{20}^{(2)} = \sqrt{\frac{3}{8}}\sin^2\theta, \quad d_{00}^{(2)} = \frac{1}{2}\left(3\cos^2\theta - 1\right) \qquad [34]. \tag{2.7}$$

This yields an expression for the quadrupole Hamiltonian in the lab frame,

$$\mathcal{H}_Q = \frac{e^2qQ}{4I(2I-1)}\left(3I_z^2 - I(I+1)\right)\frac{1}{2}\left((3\cos^2\theta - 1) + \eta\sin^2\theta\cos 2\phi\right). \tag{2.8}$$

In the presence of an applied magnetic field and an electric field gradient, the perturbation of the energy levels of a spin 1 nucleus by the quadrupolar interaction with the applied EFG is small and can be considered a first-order perturbation. The three spin 1 Zeeman energy levels are shifted by this quadrupolar interaction to

$$E_m = -\hbar\omega_0 m + \frac{e^2qQ}{4}(3m^2 - 2)\left(\frac{3\cos^2\theta - 1}{2} + \frac{1}{2}\eta\sin^2\theta\cos 2\phi\right)$$

with allowed transitions governed by the selection rule $\Delta m = \pm 1$. As shown in figure 2.1 two distinctly different transitions result. The quadrupolar splitting between the resulting two peaks in the spectrum is, in the absence of motion,

$$\Delta\nu_Q(\theta,\phi) = \frac{\omega_Q}{2\pi} = \frac{3}{2}\frac{e^2qQ}{h}\left(\frac{3\cos^2\theta - 1}{2} + \frac{1}{2}\eta\sin^2\theta\cos 2\phi\right). \tag{2.9}$$

e^2qQ/h is called the quadrupolar coupling constant. For deuterons in C-D bonds it is roughly 169 kHz [37]. Thus the separation between the two lines is much larger than

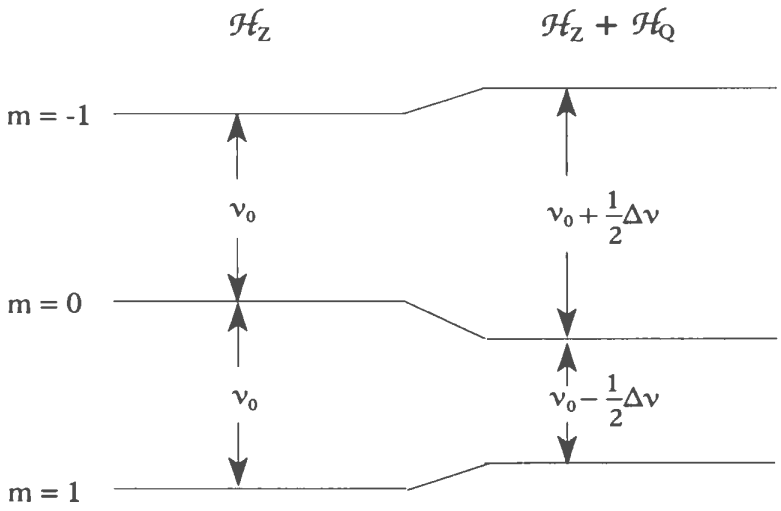

Figure 2.1: Splitting of the Zeeman energy levels by the quadrupolar interaction.

either the dipolar interaction or the chemical shift anisotropy, which are typically a few kHz. Note that

$$\Delta\nu_Q(\theta) = \frac{3}{2}\frac{e^2qQ}{h}\left(\frac{3\cos^2\theta - 1}{2}\right)$$

for the special case of an axially symmetric field gradient which has $\eta = 0$. This is approximately true of the C-D bonds in lipid acyl chains.

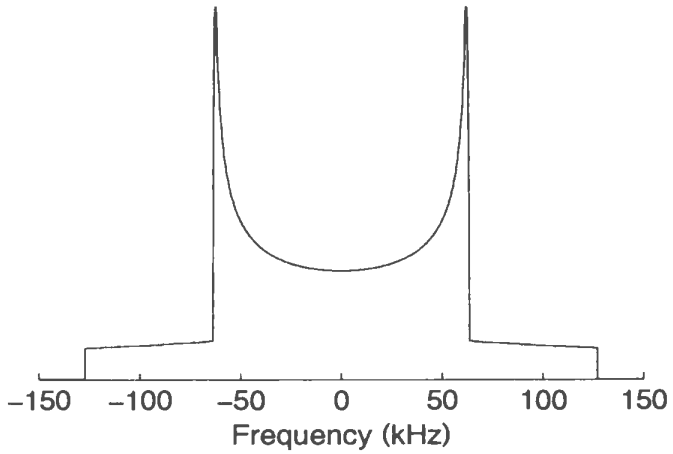

Figure 2.2: Model powder spectrum for phospholipids deuterated in a single acyl chain position. The sharp shoulders and peaks of the spectrum are broadened in real systems.

In a crystal powder all orientations of the individual crystallites, and thus of the

EFG tensor with respect to the magnetic field, are possible. Statistically we expect to find many more molecules perpendicular rather than parallel to the applied field, giving rise to a characteristic powder pattern [38]. The resulting spectrum will be the sum of two overlapping powder patterns similar in shape but opposite in sign (figure 2.2). A perpendicular orientation of the C-D bond with the magnetic field, corresponding to $\theta = 90°$, gives

$$\Delta\nu_{Q\perp} = \frac{3}{4}\frac{e^2qQ}{h} \approx 125 \text{ kHz},$$

which we identify with the separation of the two inner intense peaks in the rigid lattice spectrum. Likewise we assign the separation of the outer edges of the rigid lattice spectrum to the parallel orientation with $\theta = 0$ and

$$\Delta\nu_{Q\parallel} = \frac{3}{2}\frac{e^2qQ}{h} \approx 250 \text{ kHz}.$$

The angle θ_m corresponding to the point where the two curves cross is called the "magic angle", and is equal to 54.7° as required by the condition $3\cos^2\theta_m - 1 = 0$.

2.2 ^{2}H NMR in the Presence of Molecular Motion

In general molecules are dynamic and, depending on the timescale of the motion, the dynamics can affect the spectrum. While rapid isotropic motion gives rise to a single collapsed line in the NMR spectrum, for anisotropic motion each deuteron contributes a doublet due to the residual quadrupolar moment of the nucleus. The reduced spacing $\Delta\nu_Q$ between the peaks of the doublet is a measure of the anisotropy of the motion at that nucleus [39] and is called the quadrupole splitting. If cylindrical symmetry is assumed

for the averaged motion of a chain segment, $\Delta\nu_Q$ can be written [39]

$$\Delta\nu_Q(\theta,\phi) = \frac{3}{2}\frac{e^2qQ}{h}|S_{CD}|\left(\frac{3\cos^2\theta-1}{2}+\frac{1}{2}\eta\sin^2\theta\cos 2\phi\right), \tag{2.10}$$

label where

$$S_{CD} = \left\langle\frac{3\cos^2\beta-1}{2}\right\rangle$$

is the deuterium order parameter for the molecular motion[1]. $|S_{CD}| = 1/2$ when a chain is in the all-*trans* state and $\langle S_{CD}\rangle = 0$ for a fully disordered (isotropically tumbling) segment. β is the angle between the C-D bond and the direction of the magnetic field. The angular brackets indicate an average over those motions which satisfy $M_2\tau_c^2 \ll 1$ where M_2 is the second moment characterising the distribution of spectral frequencies in the absence of molecular motion, and τ_c is the correlation time for the motion. Molecular reorientation thus transforms the spectrum into one which is an average over the fast motions.

2.3 Density Operator Formalism

Since the aim of the theoretical analysis of NMR spectroscopy is prediction of the outcome of experiments, the solution of the Schrödinger equation should prove a fruitful approach. However, a typical NMR experiment involves on the order of 10^{20} particles which has the significant consequence that we never have a complete and deterministic specification of

[1]Separate order parameters can be written for the motion of the molecular frame and segmental motion with respect to that frame, but NMR always measures the *product* of the two; they cannot be measured independently. Petersen and Chan [7] report that a comparison of proton and deuterium order parameters can lead to an estimate of the relative importance of these two order paramaters, but in this thesis no attempt will be made to attribute changes in $\langle S_{CD}\rangle$ to variations in chain reorientation or chain isomerisation.

the quantum mechanical system. Instead the quantum mechanical observables involve statistical averages over the ensemble. The standard density matrix formalism [40] [41] is used to provide reasonable solutions for the two basic problems faced by the experimenter: what does a pulse do to the spin system, and how does the spin system evolve in the absence of rf pulses?

The Liouville - von Neumann equation of motion for the density matrix ρ, in the presence of a Hamiltonian $\mathcal{H}$, is

$$\frac{d\rho}{dt} = -\frac{i}{\hbar}[\mathcal{H}, \rho(t)] \tag{2.11}$$

and the measured value of an observable represented by the operator $\mathcal{Q}$ is

$$\langle \mathcal{Q} \rangle = Tr\{\mathcal{Q}\rho\}. \tag{2.12}$$

$\rho(t)$ is the density matrix in a frame which rotates at the frequency of the applied field ω_1. Although this formalism provides a rigorous description of the time evolution of a nuclear spin system, for anything but the simplest case the matrix calculations quickly become unwieldy.

An operator formalism is constructed to make the calculations tractable. For a general isolated spin system $\rho(t)$ can be written in terms of the unit operator and a set of n orthonormal Hermitian operators denoted by $\overline{\mathbf{p}}$ where p takes on the values $1, 2, 3, \ldots, n$.

$$\rho(t) = \overline{\mathbf{1}}_{op} + \sum_{p}^{n} c_p(t)\overline{\mathbf{p}} \tag{2.13}$$

such that the trace of any two of these operators $Tr\{\overline{\mathbf{p}}\,\overline{\mathbf{q}}\} = \delta_{pq}$. For a spin 1 system $n = 8$ and we must choose a set of eight Hermitian operators based on the Hamiltonians

of interest. Given that

$$\mathcal{H}_x = -\hbar\omega_1 I_x \quad \text{and} \quad \mathcal{H}_y = -\hbar\omega_1 I_y$$

during pulses applied along the x and y axes in the rotating frame, and

$$\mathcal{H}_Q = \hbar\frac{\omega_Q}{3}\left(3I_z^2 - 2\right)$$

in the absence of rf pulses, it is reasonable to choose a basis set in terms of the spin operators I_x, I_y and I_z

$$\overline{\mathbf{1}} = \frac{I_x}{\sqrt{2}} \quad \overline{\mathbf{2}} = \frac{I_y}{\sqrt{2}} \quad \overline{\mathbf{3}} = \frac{I_z}{\sqrt{2}}$$

$$\overline{\mathbf{4}} = \frac{1}{\sqrt{6}}\left(3I_z^2 - 2\right)$$

$$\overline{\mathbf{5}} = \frac{1}{\sqrt{2}}\left(I_xI_z + I_zI_x\right) \quad \overline{\mathbf{6}} = \frac{1}{\sqrt{2}}\left(I_yI_z + I_zI_y\right)$$

$$\overline{\mathbf{7}} = \frac{1}{\sqrt{2}}\left(I_x^2 - I_y^2\right) \quad \overline{\mathbf{8}} = \frac{1}{\sqrt{2}}\left(I_xI_y + I_yI_x\right). \tag{2.14}$$

following the notation of Bloom [42]. The equation of motion 2.11 in terms of the operator $\overline{\mathbf{p}}$ is

$$\frac{dc_p}{dt} = \frac{i}{\hbar}\sum_q c_q(t)\, Tr\{\overline{\mathbf{p}}\,[\mathcal{H}, \overline{\mathbf{q}}]\}. \tag{2.15}$$

The coefficients $c_p(t)$ contain all of the information necessary to describe the time evolution of the physical observable $\mathcal{Q}$. They can be represented as the vector $\mathbf{C}(t) = (c_0(t), c_1(t), c_2(t) \ldots c_s(t))$.

The Zeeman Hamiltonian and the axially symmetric part of the quadrupolar Hamiltonian (eq. 2.8) can be written using the operator $\overline{\mathbf{p}}$ as follows

$$\mathcal{H}_Z = -\hbar\omega I_z = -\sqrt{2}\,\hbar\omega_0\,\overline{\mathbf{3}} \tag{2.16}$$

$$\mathcal{H}_Q = \frac{\omega_Q}{3}\hbar\left(3I_z^2 - 2\right) = \sqrt{\frac{2}{3}}\,\hbar\omega_Q\,\overline{\mathbf{4}}. \tag{2.17}$$

Using table A.1 in appendix A the commutators for these operators can be written down by inspection. It is immediately apparent which operators are invariants of the motion and which are coupled. For the Zeeman Hamiltonian $\mathcal{H}_Z$, $\overline{\mathbf{3}}$ and $\overline{\mathbf{4}}$ are invariants and the remaining six operators are coupled in pairs: $\overline{\mathbf{1}}$ and $\overline{\mathbf{2}}$; $\overline{\mathbf{5}}$ and $\overline{\mathbf{6}}$; and $\overline{\mathbf{7}}$ and $\overline{\mathbf{8}}$. The solutions can be represented by the precession diagrams in figure A. For the axially symmetric quadrupolar interaction $\mathcal{H}_Q$, $\overline{\mathbf{3}}$, $\overline{\mathbf{4}}$, $\overline{\mathbf{7}}$ and $\overline{\mathbf{8}}$ are invariants leaving only two sets of precessing pairs: $\overline{\mathbf{1}}$ and $\overline{\mathbf{6}}$; and $\overline{\mathbf{2}}$ and $\overline{\mathbf{5}}$.

In pulsed NMR it is necessary to solve the equation of motion during the perturbation as well as during the evolution of the spin system. For a pulse applied along the x axis, $\mathcal{H}_x = -\sqrt{2}\,\hbar\omega_1\,\overline{\mathbf{1}}$ and thus the invariants are $\overline{\mathbf{1}}$ and $\frac{1}{2}\overline{\mathbf{4}} - \frac{\sqrt{3}}{2}\overline{\mathbf{7}}$. The coupled operators are shown in the precession diagrams. Similarly for a pulse applied along the y axis, $\mathcal{H}_y = -\sqrt{2}\,\hbar\omega_1\,\overline{\mathbf{2}}$ in the rotating and the invariants of the pulse are $\overline{\mathbf{2}}$ and $\frac{1}{2}\overline{\mathbf{4}} + \frac{\sqrt{3}}{2}\overline{\mathbf{7}}$. Again the coupled pairs can be seen in the precession diagrams. In appendix A it is shown how this formalism may be used to follow the role of the rf pulses and the quadrupolar interaction during a particular pulse sequence.

2.4 Quadrupole Echo

With well-designed pulse sequences it is possible to manipulate the nulear spin system Hamiltonian at will almost without restriction. One use of such control is in producing a spin echo to overcome the dead time associated with the receiver of the spectrometer [43].

In solids the ^{2}H NMR spectrum can be quite broad so that much of the information is lost before the receiver is ready to detect it after an rf pulse. This prevents the experimenter from obtaining valuable information in the initial part of the signal. The information can be recovered via application of a second pulse 90° out of phase with the first at time $t = \tau$. This reverses the dephasing of magnetisation and gives rise to an echo at $t = 2\tau$. Almost all modern pulse and multidimensional NMR experiments involve echoes.

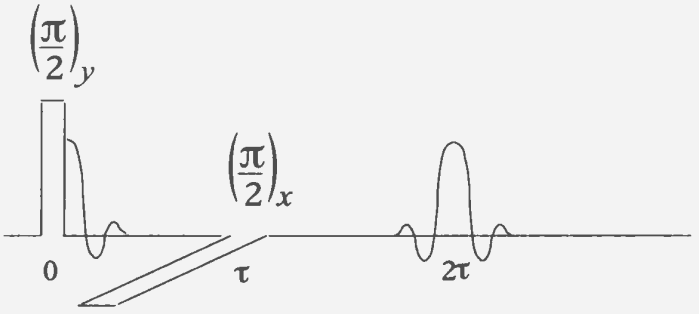

Figure 2.3: The quadrupolar echo pulse sequence. The trailing half of the echo at $t = 2\tau$ is equivalent to the free induction decay signal but for some irretrievable loss of phase memory due to transverse relaxation.

For spin 1/2 systems the pulse sequence $(\pi/2)_x - \tau - (\pi)_y - t$ is used. It is commonly called a Hahn echo and has a simple vector description. The *quadrupolar echo* pulse sequence $(\pi/2)_x - \tau - (\pi/2)_y - t$ is used for spin 1 systems [43]. It is not immediately obvious how this pulse sequence inverts the plane in which the state evolves due to the quadrupolar interaction. In appendix A the quadrupolar echo is explained using the density operator formalism described above.

The quadrupolar echo sequence is often used simply to obtain a spectrum in situations where the spectrum is broad. It is more powerful, however, in that it can be used in combination with other pulse sequences to refocus specific coherences. The technique

also lends itself to the measurement relaxation times. The trailing half of the echo at $t = 2\tau$ as calculated in equation A.18 is equivalent to the free induction decay signal [35] but for some irretrievable loss of phase memory due to motions which reorient the C-D bond during the pulse sequence.

2.5 ^{2}H Quadrupolar Relaxation

The static Hamiltonian of equation 2.1 should more precisely be written

$$\mathcal{H}_0 = \mathcal{H}_Z + \langle \mathcal{H}_Q(t) \rangle \tag{2.18}$$

where $\mathcal{H}_Z$ is the Zeeman Hamiltonian and $\mathcal{H}_Q$(t) is the time-dependent quadrupolar Hamiltonian. The quadrupolar relaxation Hamiltonian for a spin 1 system, namely the deuteron's interaction with the electric field gradient of the nucleus under the influence of molecular motion, is of the form [40] [35]

$$\mathcal{H}_Q^{relax}(t) = \mathcal{H}_Q(t) - \langle \mathcal{H}_Q(t) \rangle. \tag{2.19}$$

$\mathcal{H}_Q^{relax}(t)$ is the time-dependent part of the thermally driven quadrupolar Hamiltonian $\mathcal{H}_Q(t)$ with respect to the average value $\langle \mathcal{H}_Q(t) \rangle$. $\mathcal{H}_Q(t)$ is a randomly fluctuating function whose time-dependence is in the random functions $\theta(t)$ and $\phi(t)$, the polar and azimuthal angles of the symmetry axis of the EFG in a magnetic field along the z-axis. The fluctuations of the field at the site of the nucleus are the result of motions which change the orientation of the C-D bond.

These motions have associated with them a correlation function $G_{mm'}(t)$ expressed in terms of a scalar product of the local field $F_m(t)$ and the same local field at some

later time $F_{m'}(t')$. $G_{mm'}(t)$ is thus a measure of how rapidly the EFG (and ω_Q) is being modulated. For random motions the correlation function

$$G_{mm'}(t) \propto F_m(t)\, F_{m'}(t') \propto e^{-\tau/\tau_c}, \quad \tau = t' - \tau \tag{2.20}$$

is exponential and independent of the time origin. τ_c is called the correlation time for the motion. The Fourier transform of the correlation function

$$J_{mm'}(\omega) = \int_{-\infty}^{\infty} G_{mm'}(t) e^{-i\omega t} dt \tag{2.21}$$

is called the spectral density. Because of the inverse relationship between $G_{mm'}(t)$ and $J_{mm'}(\omega)$, slow motions with long correlation times will have large spectral densities at low frequencies.

Relaxation times are normally written in terms of spectral densities. The relationships can be derived through time-dependent perturbation theory [44] or equivalently by using the density matrix [35]. Table A.2 lists the relaxation times associated with the various spin 1 basis operators $\overline{\mathbf{p}}$. T_2 describes the decay of the transverse single-quantum coherences, and thus the quadrupolar echo amplitude, resulting from modulation of ω_Q by these motions. T_2 is written in terms of the spectral densities $J_0(0)$, $J_1(\omega_0)$ and $J_2(2\omega_0)$, and is thus sensitive to motions which randomly vary the EFG at frequencies ω_0 and $2\omega_0$, as well as very slow motions. ^{2}H NMR relaxation measurements provide an ideal means of observing slow motions in lipid bilayers.

The fluctuations of the quadrupolar interaction give rise to a random accumulation of phase which results in a decay of the quadrupolar echo. To account for relaxation,

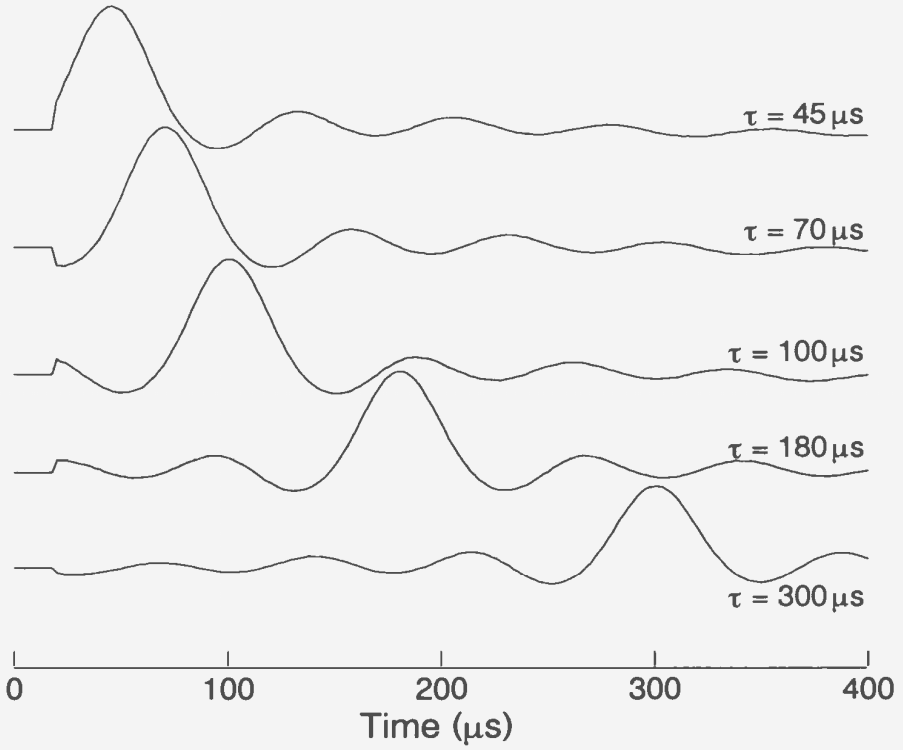

Figure 2.4: Quadrupolar echoes for a typical sample at 57°C. Time shown is for signal collected following removal of the second pulse. Note the deadtime associated with the receiver.

expression A.16 for $c_1(t)$ should be written

$$c_1(t) = I_0 \cos\left(\omega_Q \left[t - 2\tau\right]\right) e^{-2\tau/T_{2e}} \tag{2.22}$$

where T_{2e} is the effective transverse relaxation time describing the decay of the echo amplitude. The echo amplitude is measured for various values of τ as shown in figure 2.4 and fit to an exponential decay to extract T_{2e}.

2.6 Molecular Motion and Second Moments

A motion which modulates ω_Q is expected to modulate a portion, ΔM_2, of the second moment of the spectrum [9]. Hence T_{2e} may be interpreted in terms of the change in M_2 [40]. For fast motions which contribute to motional narrowing, $T_{2e} \approx T_2$ and the change

in the observed second moment is

$$\Delta M_2 = \langle \omega^2 \rangle - \langle \omega \rangle^2 = \langle (\Delta\omega)^2 \rangle, \tag{2.23}$$

the mean square fluctuation in the quadrupolar splitting. Adiabatic motions are too slow to contribute to motional averaging and only gradually modulate the orientation-dependent quadrupolar splittings. For slow motions, $1/T_{2e}$ is the effective quadrupolar echo decay rate and the observed second moment is M_{2r}, the *residual second moment* of the spectrum [45]:

$$M_{2r} = M_2 - \langle (\Delta\omega)^2 \rangle. \tag{2.24}$$

Pauls *et al.* [46] have defined the relationships between T_{2e}, ΔM_2 and the correlation time, τ_c, for the limiting cases of fast and slow motions. For fast motions which contribute to motional narrowing,

$$\Delta M_2 \tau_c \ll 1 \quad \text{and} \quad \frac{1}{T_{2e}} = \Delta M_2 \tau_c, \tag{2.25}$$

while for slow motions which do not contribute to motional narrowing,

$$M_{2r} \tau_c \gg 1 \quad \text{and} \quad \frac{1}{T_{2e}} \propto \frac{1}{\tau_c}. \tag{2.26}$$

Since $1/T_{2e} \propto \tau_c$ for fast motions while $1/T_{2e} \propto 1/\tau_c$ for slow motions, the value of T_{2e} must go through a minimum for intermediate values of τ_c.

3

Acyl Chain Order in DPPG/DPPC Mixtures

3.1 ^{2}H-NMR Spectra

A ^{2}H-NMR spectrum of the fully-hydrated chain-perdeuterated phospholipid is a superposition of axially averaged powder patterns arising from the different deuterons for the various CD_2 segments along the acyl chains and the terminal CD_3 segment. For fluid membranes the molecular motions are axially symmetric and the normal to the bilayer is the axis of symmetry. The quadrupolar splitting of each powder pattern is given by equation 2.10

$$\Delta\nu_Q(\theta,\phi) = \frac{3}{2}\frac{e^2qQ}{h}|S_{CD}|\left(\frac{3\cos^2\theta-1}{2}\right),$$

where ϕ describes the orientation of the C-D bond with respect to the bilayer normal and θ is the angle between the bilayer normal and the static magnetic field. The deuteron order parameter S_{CD} reports on the average conformation of the phospholipid molecule and the amplitude of the motions of the corresponding CD bond. The order parameter $\langle S_{CD}\rangle$ averaged over all the deuterons in the sample thus provides time-averaged structural information about the membrane system.

A deuterium spectrum typical of a liquid crystal bilayer conformation is shown in figure 3.1. Figure 3.1 also shows the spectrum corresponding to an oriented sample where

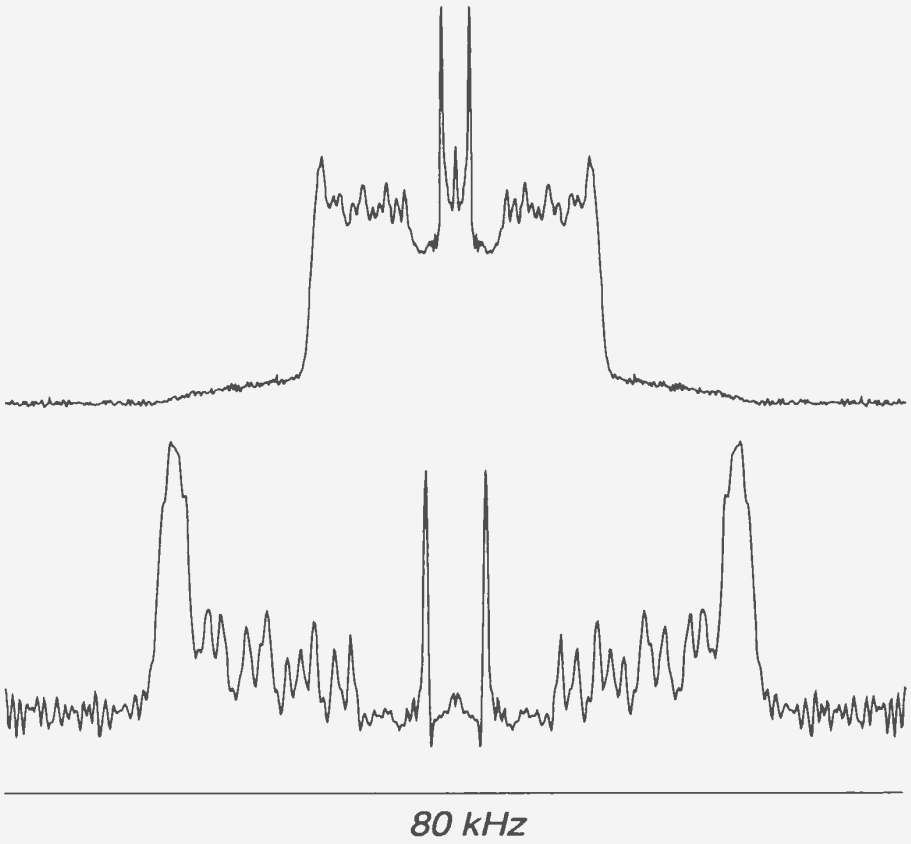

Figure 3.1: ^{2}H-NMR spectrum of DPPC-d_{62} at 60°C. The powder spectrum is shown on top and the corresponding dePaked spectrum, calculated from the powder spectrum, is shown on the bottom.

the bilayer normal is parallel to the field ($\theta = 0$). Analytical dePakeing of spectra [47] [48] was used to separate the superimposed peaks and obtain oriented spectra. Near the outer edges of the dePaked spectrum there is an overlapping of the quadrupolar splittings corresponding to roughly seven CD_2 segments closest to the glycerol backbone. Further away from the glycerol backbone the acyl chains experience progressively more motional freedom, giving rise to well-resolved peaks. The terminal methyl groups experience the greatest degree of motional freedom and thus correspond to the smallest quadrupolar splittings.

The first moment of the spectrum M_1 is directly related to $\langle S_{CD} \rangle$ and so is used as a

measure of chain order:

$$M_1 = \frac{\pi}{\sqrt{3}} \frac{e^2 qQ}{h} \langle S_{CD} \rangle. \tag{3.1}$$

M_1 represents a sum over the quadrupolar splittings [49]

$$M_1 = \frac{\int_0^\infty f(\nu)\, \nu \, d\nu}{\int_0^\infty f(\nu)\, d\nu} \tag{3.2}$$

and can be calculated directly from the spectrum. Because the odd moments of a symmetric spectrum will be zero, it is customary to take the moments of the half-spectrum. The nature of the data collection dictates that the spectrum obtained from a fast Fourier transform (FFT) of the time series data will be a discrete rather than continuous function. Equation 3.2 then becomes the weighted harmonic average over the N points of the half-spectrum;

$$\langle M_1 \rangle = \frac{\sum_{j=1}^{N} F(\nu_j)\, \nu_j}{\sum_{j=1}^{N} F(\nu_j)}. \tag{3.3}$$

The temperature dependence of M_1 can also provide information about phase behaviour. When phospholipids undergo a phase transition from liquid crystalline to gel there is a dramatic change in the spectrum, as demonstrated in figure 3.2 for pure DPPC-d_{62}. The molecular motions which determine the shape of the spectrum in the fluid phase are rapid axially symmetric motions, while the gel phase spectrum is dominated by slow, axially asymmetric motions [31] [50].

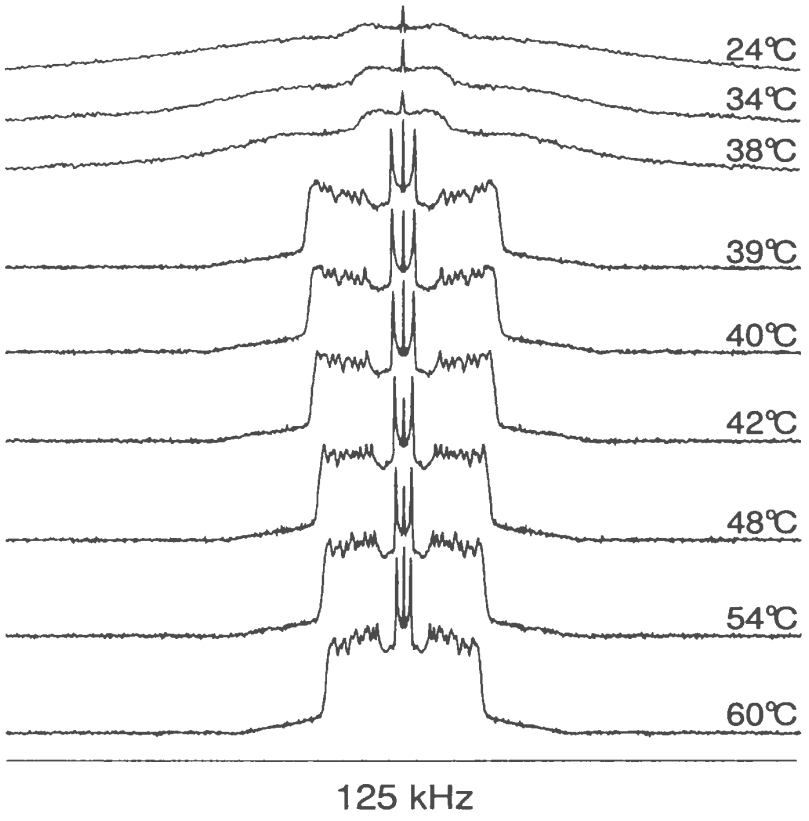

Figure 3.2: Temperature dependence of pure DPPC-d_{62}.

3.2 Results and Discussion

The first question addressed is how calcium affects the phase transition and chain order of pure DPPC-d_{62}. As demonstrated in figure 3.3 for pure DPPC-d_{62} Ca^{2+} induces a slight shift in the transition temperature. The presence of calcium has little effect on chain order in either the liquid crystal or the gel phase of chain-perdeuterated DPPC.

The effect of DPPG on the thermotropic behaviour and chain order of DPPC in the absence of calcium was also investigated. In figure 3.4 each of the samples exhibits a sharp phase transition and there is no evidence of two-phase coexistence. There is a slight shift in transition temperature and the small difference in spectral moments in

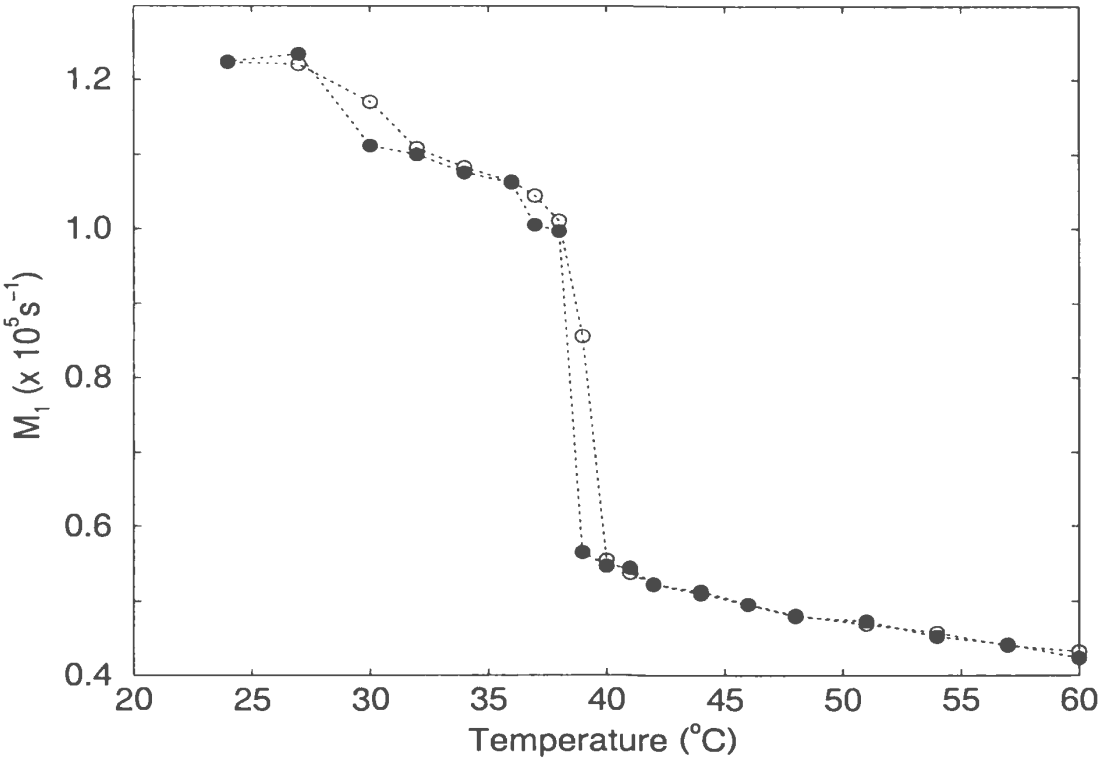

Figure 3.3: M_1 order parameter temperature profiles for pure DPPC-d_{62} samples prepared in the absence (●) and presence (○) of Ca^{2+}.

the liquid crystal regime is indicative of some limited effect on chain order above T_m for these samples. Interestingly, the observed spectral moments for the pure DPPC sample are higher than those for samples containing 30% and 50% DPPG. This reflects a tighter packing of the phosphocholine moiety despite its larger steric size compared with that of the glycerol residue. A possible explanation is that a headgroup carrying a negative charge can more easily form hydrogen bonds, as proposed by Sixl and Watts [29]. It would presumably have many water molecules associated with it, resulting in a larger effective area per lipid. The perturbing effect of one lipid headgroup on the other in this case may arise from *direct* molecular interactions or be mediated through hydrogen bonding or structural changes in the water layer at the membrane surface, or quite possibly both.

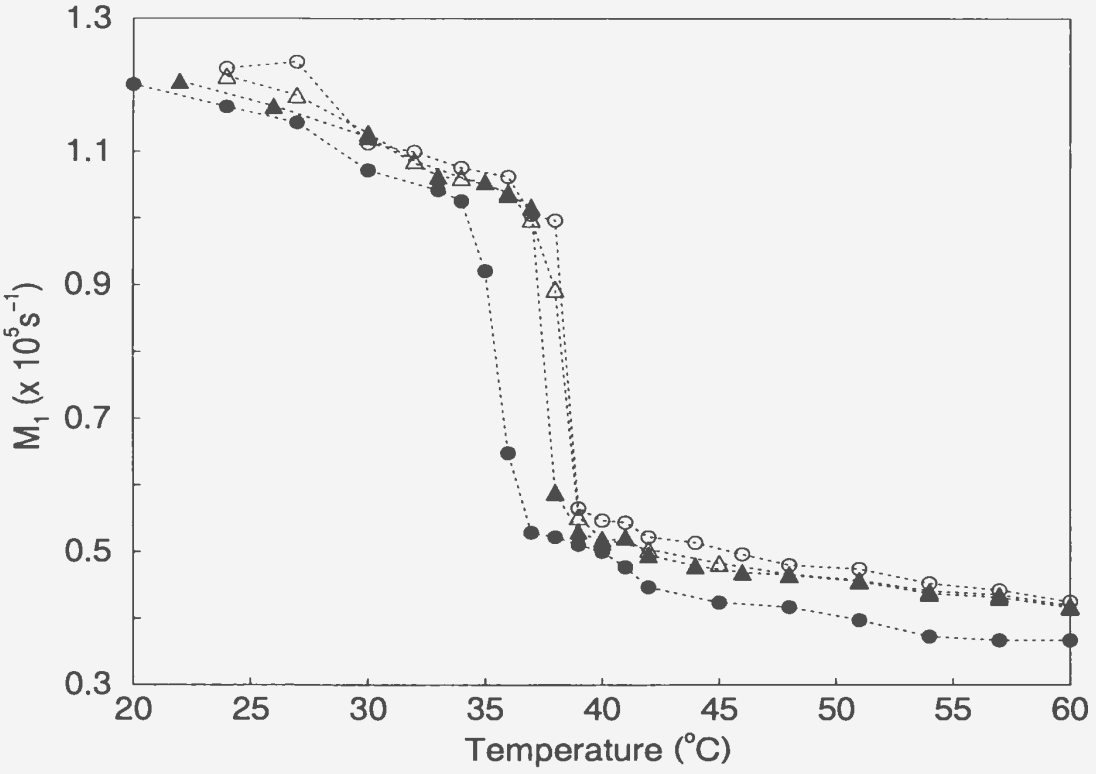

Figure 3.4: M_1 order parameter temperature profiles for mixtures of chain perdeuterated DPPC and DPPG in the absence of Ca^{2+}. The negatively charged DPPG-d_{62} component in the samples is 0% (○), 30% (△), 50% (▲) and 100% (●).

A different behaviour is observed for corresponding mixtures of chain perdeuterated DPPC and DPPG with Ca^{2+} present in the hydrating buffer. In this series of samples the mole fraction of the DPPG moiety was varied while the total number of available Ca^{2+} ions was kept constant. The results in figure 3.5 show an increasing shift to higher transition temperatures with increasing proportion of the negatively charged lipid. This suggests that in the presence of calcium ion DPPG has an ordering effect on the acyl chains of both lipids in the liquid crystal phase. The interaction of Ca^{2+} may interrupt the network of hydrogen bonding that most probably occurs through water molecules across the bilayer surface. Such molecular disruption at the membrane surface may also

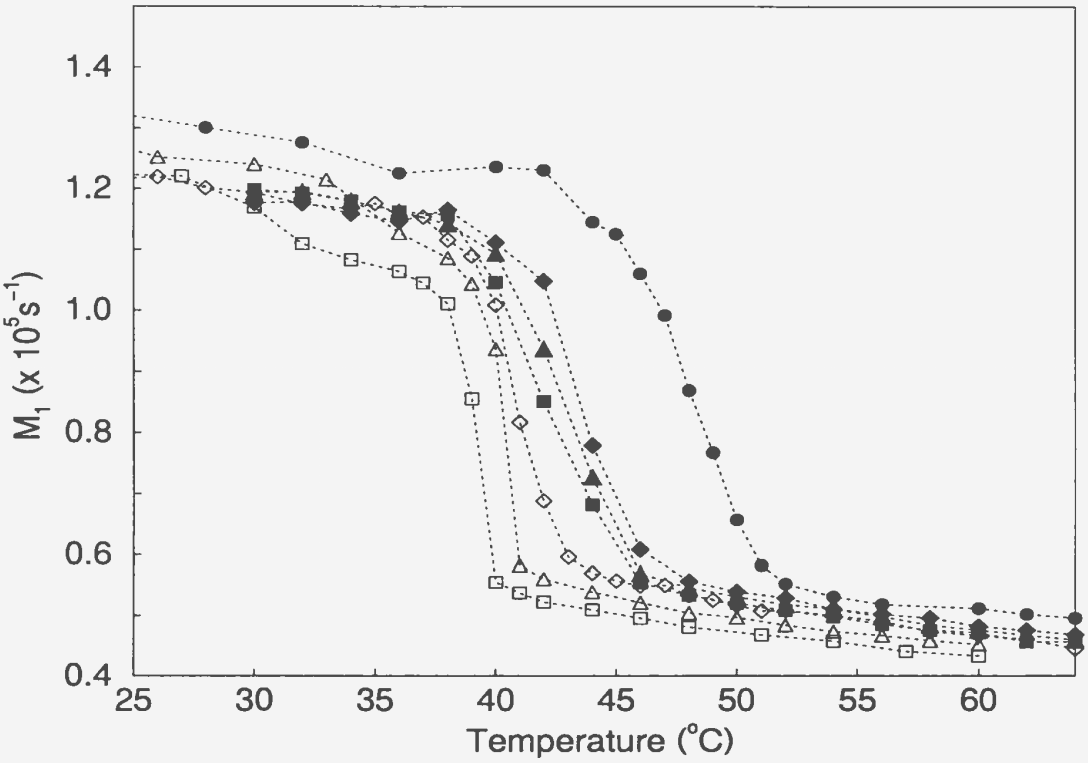

Figure 3.5: Order parameter temperature profiles for 0% (□), 7% (△), 15% (◇), 25% (■), 30% (▲), 35% (◆) and 50% (●) DPPG in DPPC in the presence of calcium ion.

increase the density in the hydrocarbon chain region and contribute to the shift of the bilayer gel to liquid-crystalline phase transition to higher temperatures.

For temperatures straddling the broadened transition region these samples exhibit coexistence of liquid crystal and gel phases. For example, between 45°C and 42°C the spectra for 35% DPPG-d_{62} in DPPC-d_{62} are superpositions of components from lipids in gel and fluid domains, as shown in figure 3.6. The narrowness of the transitions indicates that the lipids are melting together and are randomly mixed.

As the temperature is lowered in this two-phase region, gel phase domains grow at the expense of fluid phase domains [51]. The fraction of the lipids in the gel phase thus increases while the fluid phase fraction decreases. If lipids are not rapidly diffusing between

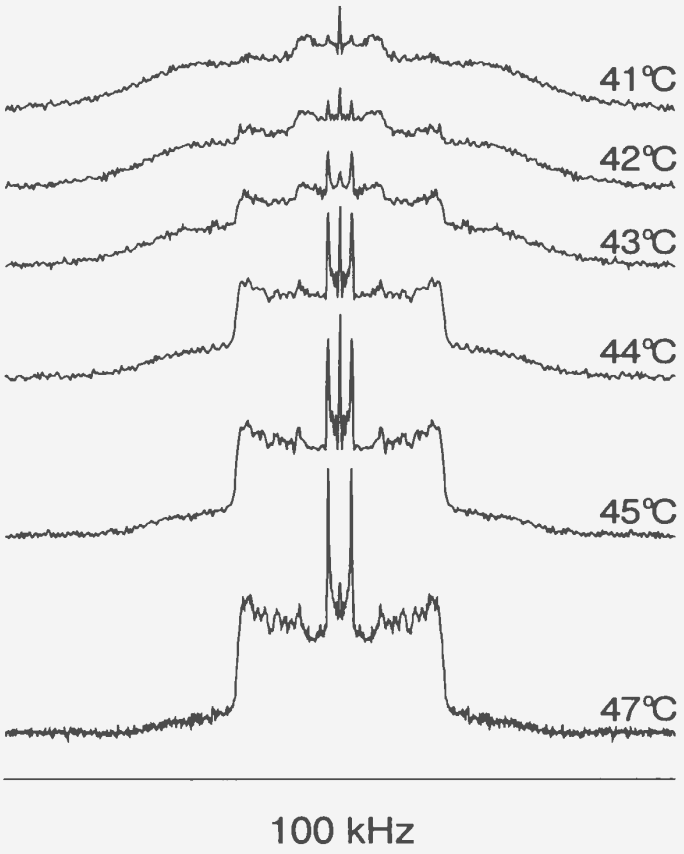

Figure 3.6: Spectra for 35% DPPG-d_{62} in DPPC-d_{62} for temperatures spanning the phase transition. These spectra exhibit coexistence of gel and fluid phases.

gel and fluid domains, the relative size of the domains should be accurately reflected in the relative intensities of the gel and fluid phase contributions to the spectrum. The two-component spectra were used to obtain a partial phase diagram for DPPC/DPPG in Ca^{2+}, shown in figure 3.7. This estimation of phase boundaries by inspection of the spectra is less rigorous than the technique used by Huschilt *et al.* [52] to derive phase diagrams. The assumption is made that the process of exchange between domains has negligible effect on the spectrum. Since the phase transition for pure DPPG occurs at 86°C, it is not possible to extrapolate the phase diagram to significantly higher DPPG concentrations.

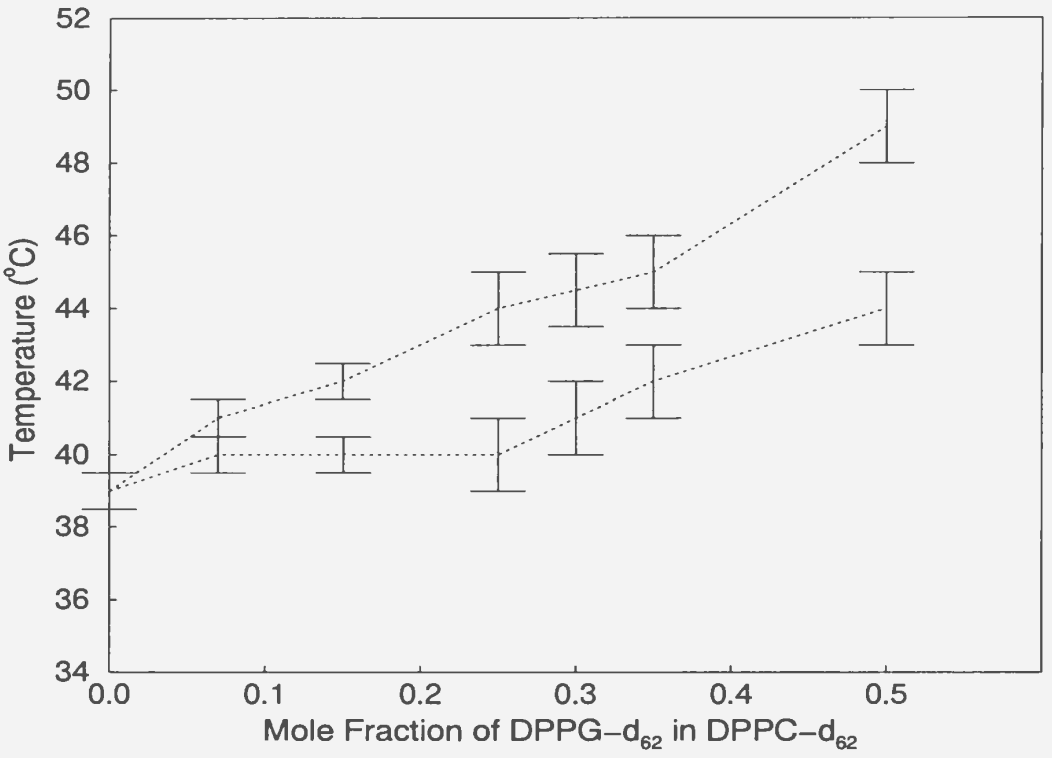

Figure 3.7: Partial phase diagram for DPPC/DPPG in 10 *mM* Ca^{2+}. Gel and liquid crystal coexist in the region between the two boundaries. The region above the two-phase region is liquid crystal and that below is gel.

Given the charged nature of the anionic headgroups and the divalent cations, the question arises as to whether Ca^{2+} is interacting with both DPPC and DPPG, or preferentially with DPPG so that the effect observed on DPPC is an indirect result of the subsequent altered environment it experiences. In the latter case a Ca^{2+}-induced change in headgroup orientation of the anionic lipid and expulsion of some of the surrounding water molecules in its hydration layer could conceivably introduce further steric constraints on both headgroups and side chains of neighbouring lipids via a reduced area per lipid. While DPPC may not form a specific complex with Ca^{2+}, Seelig *et al.* have shown that its headgroup orientation is sensitive to the bilayer surface charge [53] [16]. A change in its orientation might also result in a smaller area per headgroup and tighter packing

of the lipid chains. However, in figure 3.3 it was observed that the order parameters for pure DPPC with Ca^{2+} are almost exactly superimposed on those for the sample without calcium in the L_α region. This is striking since, if Ca^{2+} is perturbing the headgroup orientation of DPPC, it is not perturbing the acyl chains, or at least not altering the amplitude of their motions.

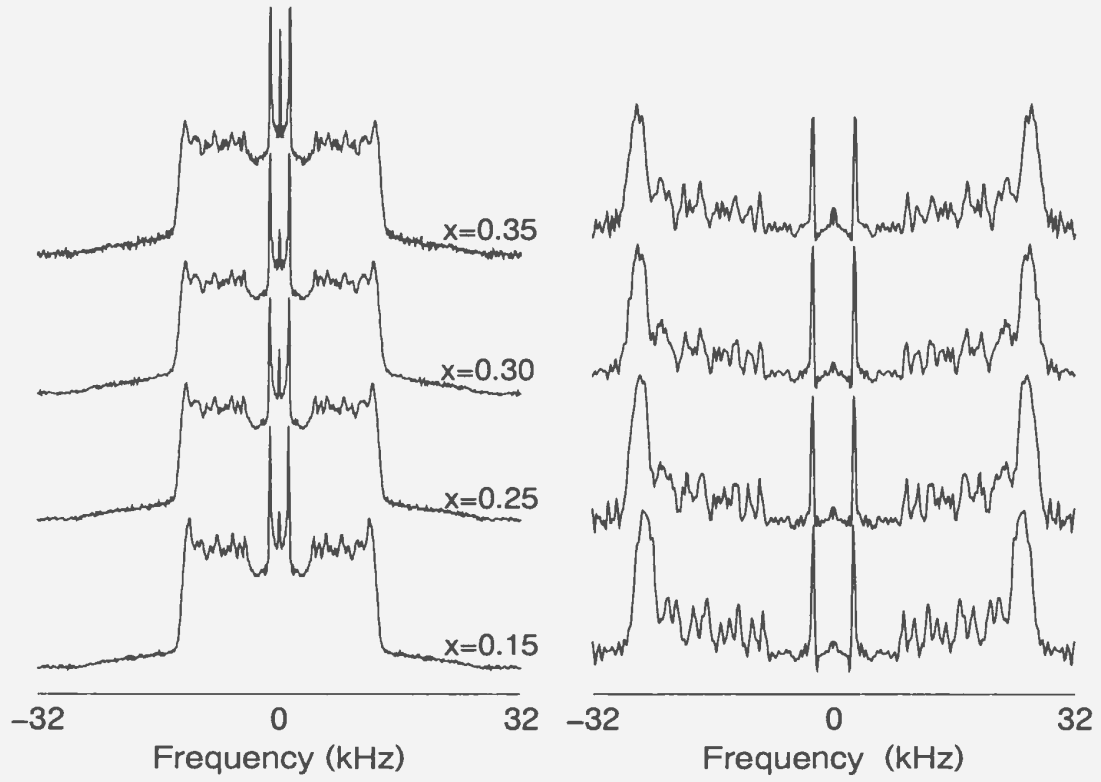

Figure 3.8: ^2H NMR spectra of DPPC-d_{62}/DPPC-d_{62}/Ca^{2+} multilamellar dispersions at 60°C as a function of the negatively-charged component. The powder spectra are shown on the left with the corresponding dePaked spectra, calculated from the powder spectra, shown on the right. The mole fraction of the anionic lipid is indicated.

If Ca^{2+} associates preferentially with the anionic lipid then we might expect DPPC and DPPG to behave differently in the mixtures. ^2H NMR spectra for mixtures with both lipids deuterated are shown in figure 3.8. The powder spectra on the left are characteristic of axially symmetric motion in liquid crystalline environments. There

is no observable separation of liquid crystalline DPPG-Ca^{2+} domains which would be expected to contribute a broad signal. The dePaked spectra display the same number of resolvable splittings as would be seen for DPPC-d_{62}. This indicates that the DPPC-d_{62} and DPPG-d_{62} chains are effectively indistinguishable in the mixture and suggests that there is no Ca^{2+}-induced phase separation for these concentrations. The complete miscibilty of DPPG-d_{62} and DPPC-d_{62} witnessed in the samples under study leads us to assume that the membrane charges are uniformly distributed over the surface.

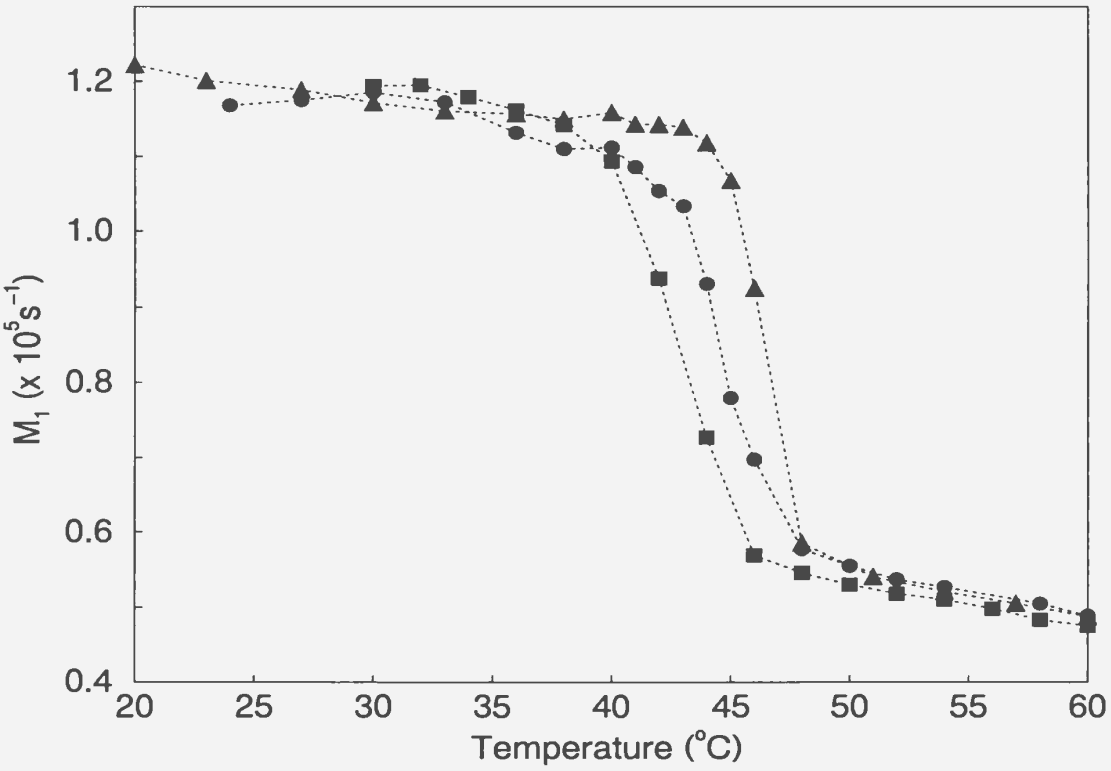

Figure 3.9: Isotopic substitution effects for samples containing 30% DPPG in DPPC with calcium ion present. M_1 order parameter temperature profiles are shown for DPPG/DPPC-d_{62} (●), DPPG-d_{62}/DPPC (▲), and DPPG-d_{62}/DPPC-d_{62} (■) mixed bilayers.

Since the timescale of ^{2}H NMR is $\approx 10^{-6}s$, the quadrupole splittings are mainly

determined by the average conformations of the phospholipid molecules and the amplitudes of the motions of the individual segments. There are contributions to the ^{2}H NMR spectrum from all deuterated lipids. The experimenter is thus prevented from observing Ca^{2+}-induced effects on individual lipids. It is possible, however, to obtain information about the average environment sampled by lipids of one type by selecting the component to be isotopically substituted. In figure 3.9 the first spectral moments are plotted for lipid mixtures containing 30% DPPG component with one or both lipids deuterated. The result that the phase transition of the sample with both lipids deuterated is lower than that with either the anionic lipid or the zwitterionic lipid deuterated, and is not an average of the two, can be explained by the shift in transition temperature introduced by isotopic substitution. The transition temperature is 41°C for the nondeuterated forms of DPPC and DPPG as opposed to 37°C for the deuterated species [54]. The differences in T_m observed here can be attributed to the amount of isotopically substituted probe molecule present, and *not* to different environments sampled by the DPPC and DPPG. The samples exhibit similar chain order in the liquid crystalline and gel phases. These results do not support a preferential association of Ca^{2+} with the DPPG headgroup or segregation into domains rich in DPPG or DPPC.

Figure 3.10 shows the first spectral moments for successive heating and cooling cycles of 30% DPPG-d_{62} in DPPC-d_{62} in calcium. The order parameters exhibit no dependence on the thermal history of the sample. Cycling the temperature does not appear to affect the packing of the lipids in the mixed bilayers. In figure 3.11 the order parameters are compared for mixtures containing 30% DPPG-d_{62} in DPPC-d_{62} in calcium, prepared

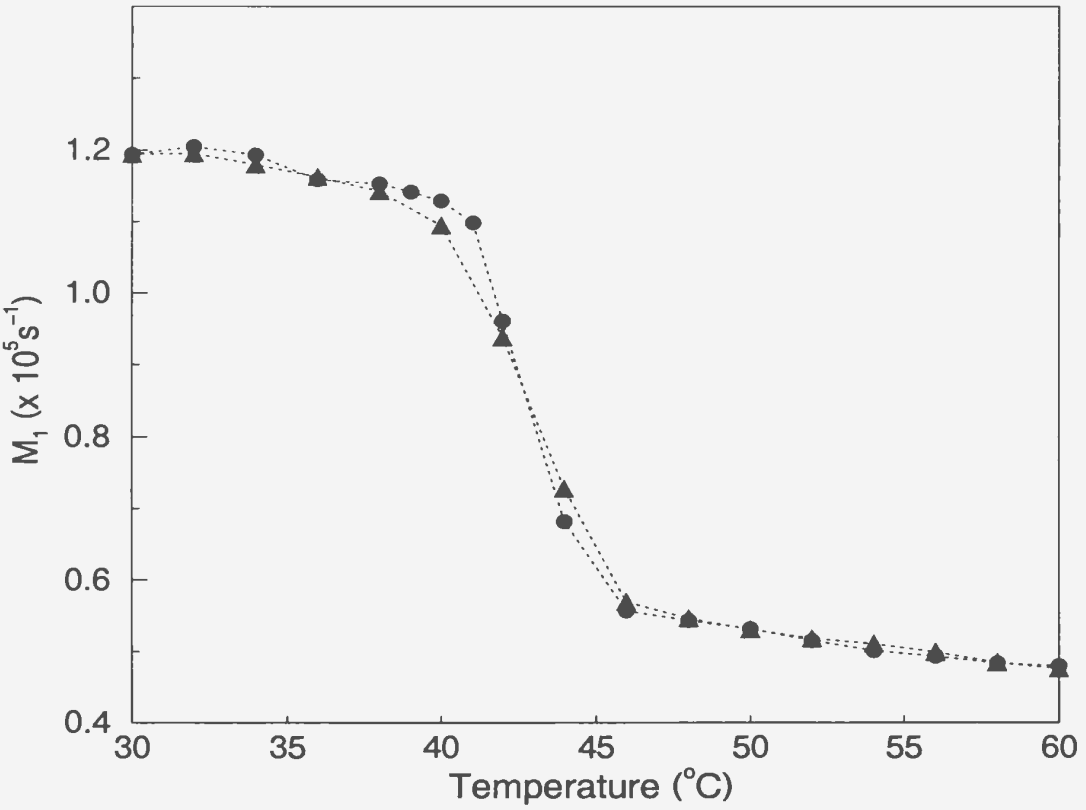

Figure 3.10: M_1 order parameters for the first cooling run (●) of 30% DPPG-d_{62} in DPPC-d_{62} mixed bilayers hydrated in the presence of Ca^{2+}; (▲) indicate the effect of successive heating and cooling.

using the two different hydration protocols. There was no appreciable difference in acyl chain order in either the L_α or the L_β phase for the two samples. The results shown in figures 3.10 and 3.11 indicate that ordering of the acyl chains in the mixtures is independent of the thermal history and method of preparation of the sample. This will be contrasted with the results for the quadrupole echo decay in chapter 4.

3.2.1 Summary

The presence of calcium causes the main transition of DPPG-d_{62}/DPPC-d_{62} mixed bilayers to shift upward and broaden. The effect is increasingly manifest with increasing

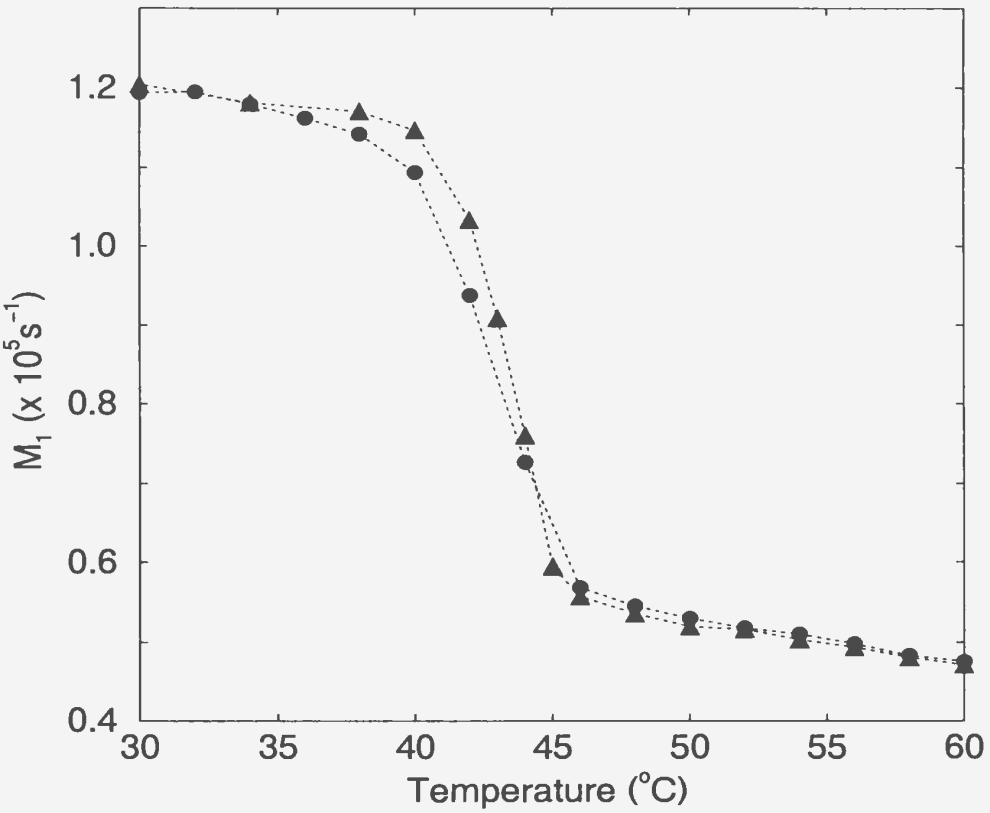

Figure 3.11: Order parameters for 30% DPPG-d_{62} in DPPC-d_{62} prepared via gentle stirring lipids in buffer (●) and rotating buffer in flask above T_m (▲). Both samples contained Ca^{2+}.

proportion of the glycerol component in the mixtures. The acyl chains are thus sensitive to the bilayer surface charge. When calcium is absent from the hydrating buffer the chains are insensitive to the bilayer surface charge. The mode of interaction of DPPG with DPPC in the absence of calcium may be predominantly a headgroup interaction, while in the presence of calcium the acyl chains are also affected. This may be due to a Ca^{2+}-induced change in the headgroup orientation, or to the exclusion or extrusion of water molecules resulting in increased order of the acyl chains. DPPG and DPPC behave similarly in the mixtures. There is no evidence of phase separation into pure DPPG or DPPC domains. The observed effects are consistent with previous results. In

a ^{2}H NMR study of the effects of divalent cations on acyl chain ordering in 5 : 1 mixtures of DPPC-d_{62}:DPPG and DPPC:DPPG-d_{62} by Zidovetski *et al.* [30], the lipids were observed to be well-mixed and no phase separation was detected. The acyl chains of both lipids experienced ordering effects in the presence of Ca^{2+}.

4

Acyl Chain Dynamics in DPPG/DPPC Mixtures

Interactions in the headgroup region might be expected to influence not only the acyl chain order, but also the motions of the acyl chains at the ^{2}H NMR timescale. When the timescale of the motion is comparable to the inverse spectral width it is possible to get information on how different motions depend on the physical state of the bilayer.

Transverse ^{2}H spin relaxation measurements were carried out by applying quadrupolar echo pulse sequences. Quadrupolar echo decay rates were measured as a function of temperature. All the quadrupolar echo decays were adequately fitted by a single exponential function of the pulse spacing τ. In determining rates using the initial slopes of the decay curves, we are implicitly averaging the relaxation behaviour over orientation and position along the chain. The deuteron transverse relaxation times in the liquid crystal bilayers exhibited some dependence on sample preparation.

4.1 Results and Interpretation of the T_{2e} Measurements

Motions are characterised by correlation times. The lipid acyl chains undergo an array of motions as discussed in section 1.1.2. The calculation of correlation times from deuteron T_{2e} values is not always straightforward [55] because the different motional modes and

their relative contribution to the modulation of ω_Q are not well-understood.

In section 2.6 it was noted that $1/T_{2e} \propto \tau_c$ for fast motions and $1/T_{2e} \propto 1/\tau_c$ for adiabatic motions. The rates of motion are additive and the measured value of T_{2e} really reflects a combination of contributions from motions of the acyl chains covering a range of timescales. A single relaxation time is insufficient to determine a molecular motion. For a given temperature some motions are much more effective than others in modulating the quadrupolar interaction, and are said to dominate T_{2e}. The correlation times for thermally activated motions increase as the sample temperature is decreased. Variation of the sample temperature can be used to separate the various types of motions [49].

As the temperature of the sample is decreased, the correlation time for some motions may become long enough that $\Delta M_2 \tau_c^2 \approx 1$. At the transition they suddenly become effective in modulating the quadrupolar interaction. This results in a large increase in the echo decay rate which often accompanies the chain-melting transition. Upon further cooling below the transition temperature the correlation times for most relevant motions pass into the regime where $1/T_{2e} \propto 1/\tau_c$ and the decay rate now decreases as the temperature is reduced. Thus T_{2e} passes through a minimum as the lipid molecules pass through the liquid crystal-to-gel transition temperature.

In the gel phase, if faster motions are slowed down sufficiently that they become important for transverse relaxation, T_{2e} may tend towards a second minimum. Motions which are the most likely candidates for an observed second T_{2e} minimum are rotational diffusion and rapid *trans-gauche* isomerisation in the hydrocarbon chains. Upon cooling below T_m, the values of τ_J, the correlation time for isomerisation, remain largely

independent of temperature [8]. This implies that they are not frozen out at the main transition.

4.2 Results and Discussion

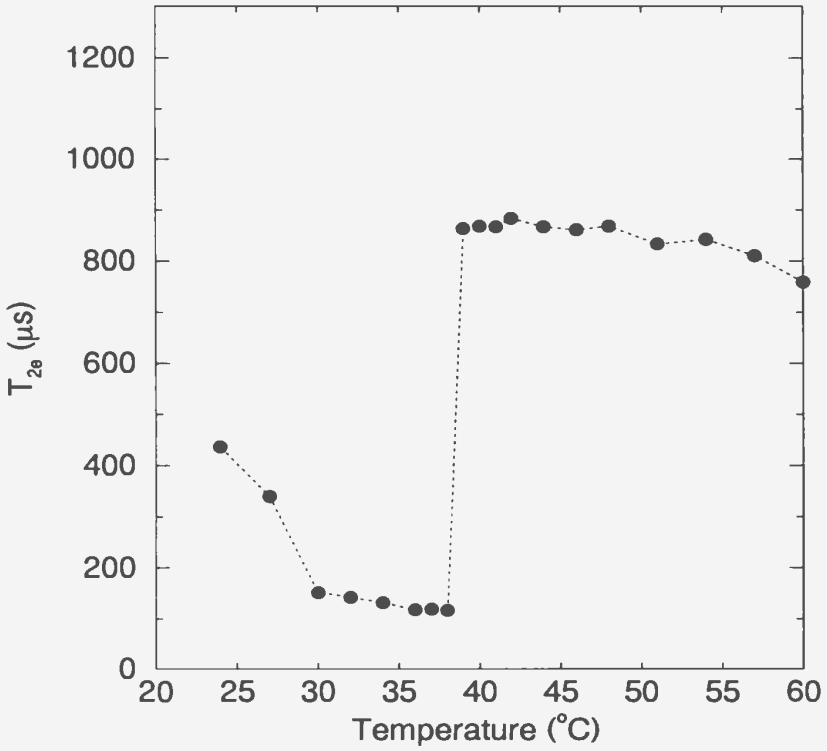

Figure 4.1: Temperature dependence of T_{2e} for DPPC-d_{62} in the absence of calcium. Values of T_{2e} were calculated from decay curves of the quadrupolar echo amplitude.

Figure 4.1 shows the deuteron transverse relaxation times for pure DPPC-d_{62} in the absence of calcium. The temperature profile of T_{2e} is typical of pure DPPC. A plateau is observed for T_{2e} in the liquid crystalline phase which may mean that this phase is dominated by at least two motions with correlation times τ_1 and τ_2 such that $\Delta M_2 \tau_1^2 \ll 1$ and $M_{2r}\tau_2^2 \gg 1$, i.e. fast and slow motions which have opposite contributions to $1/T_{2e}$. The adiabatic motions which dominate T_{2e} in this phase freeze out when the lipid bilayer

undergoes a transition to the gel phase. These motions are most likely motions which occur over large length scales, such as translational diffusion around vesicle surfaces and collective modes of the bilayers.

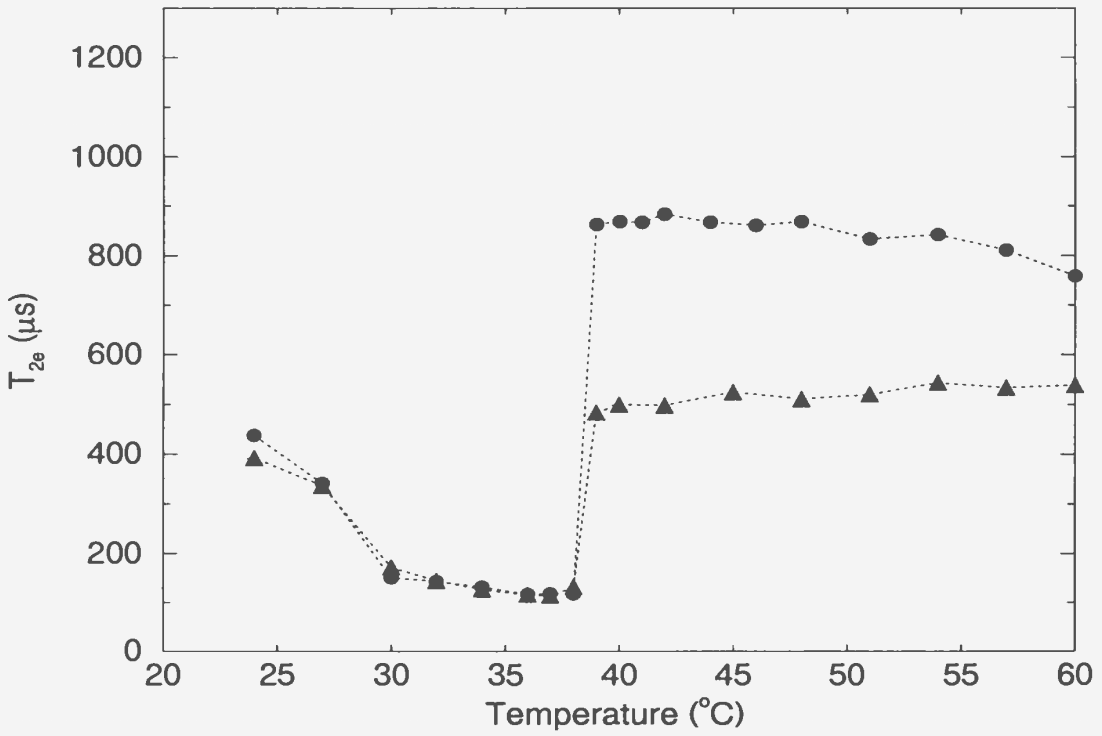

Figure 4.2: Temperature dependence of T_{2e} for pure DPPC-d_{62} (●) and 30% DPPG-d_{62}/70% DPPC-d_{62} mixed bilayers (▲) in the absence of calcium.

Figure 4.2 shows that the addition of DPPG-d_{62} to DPPC-d_{62} substantially alters deuteron transverse relaxation in the liquid crystal but not the gel phase of these bilayer systems. This suggests that the interaction of DPPG with DPPC bilayers perturbs the slow collective or diffusive motions which are responsible for transverse relaxation in the liquid crystal regime and are frozen out at the chain-melting transition. The addition of DPPG does not affect the more local motions which dominate the decay in the gel phase. The behaviour in the liquid crystal phase may be sensitive to sample preparation. This

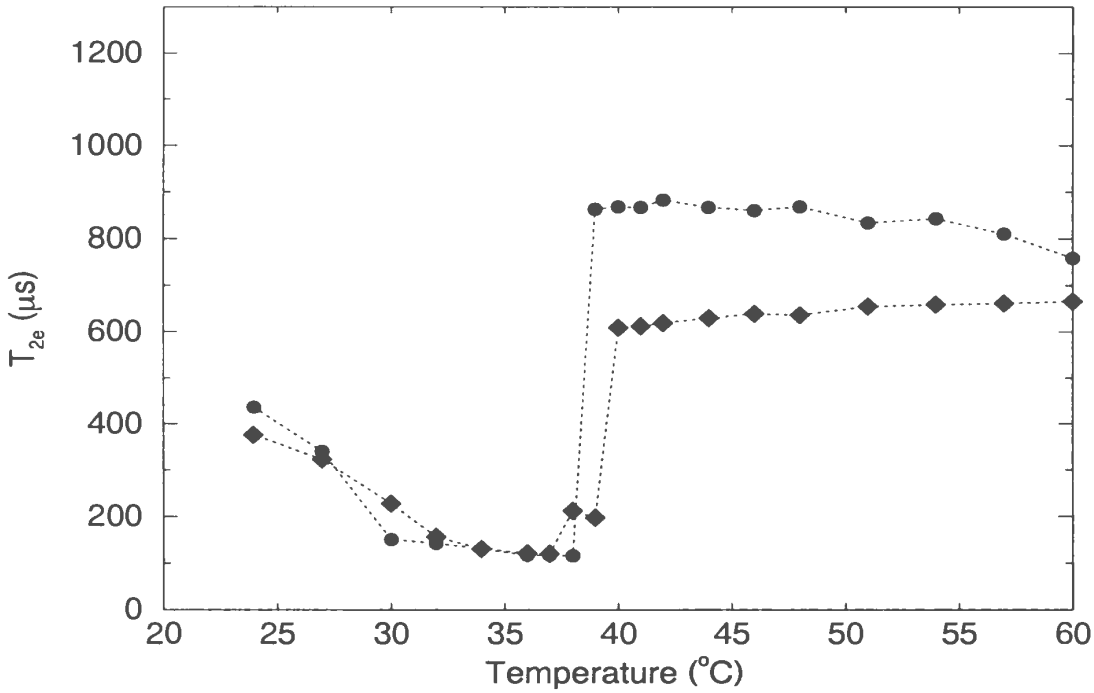

Figure 4.3: Temperature dependence of T_{2e} for DPPC-d_{62} bilayers hydrated in the presence (◆) and absence (●) of Ca^{2+}.

will be addressed below.

Calcium affects the motions which dominate the quadrupolar echo decay in the liquid crystal phase for pure DPPC. In figure 4.3 we observe no substantial effect in the gel phase of pure DPPC with the addition of calcium. The calcium ion may have a perturbing influence on a hydrogen-bonding network at the surface of pure DPPC.

The transverse relaxation time exhibited some dependence on thermal history in the binary lipid mixtures under study. Figure 4.4 shows the T_{2e} temperature profile for 30% DPPG-d_{62} in DPPC-d_{62} with Ca^{2+} present in the hydrating buffer. For successive heating and cooling cycles the T_{2e} plateau is observed to progress towards lower values, corresponding to longer correlation times.

Figure 3.11 showed that the orientational order of the acyl chains was insensitive

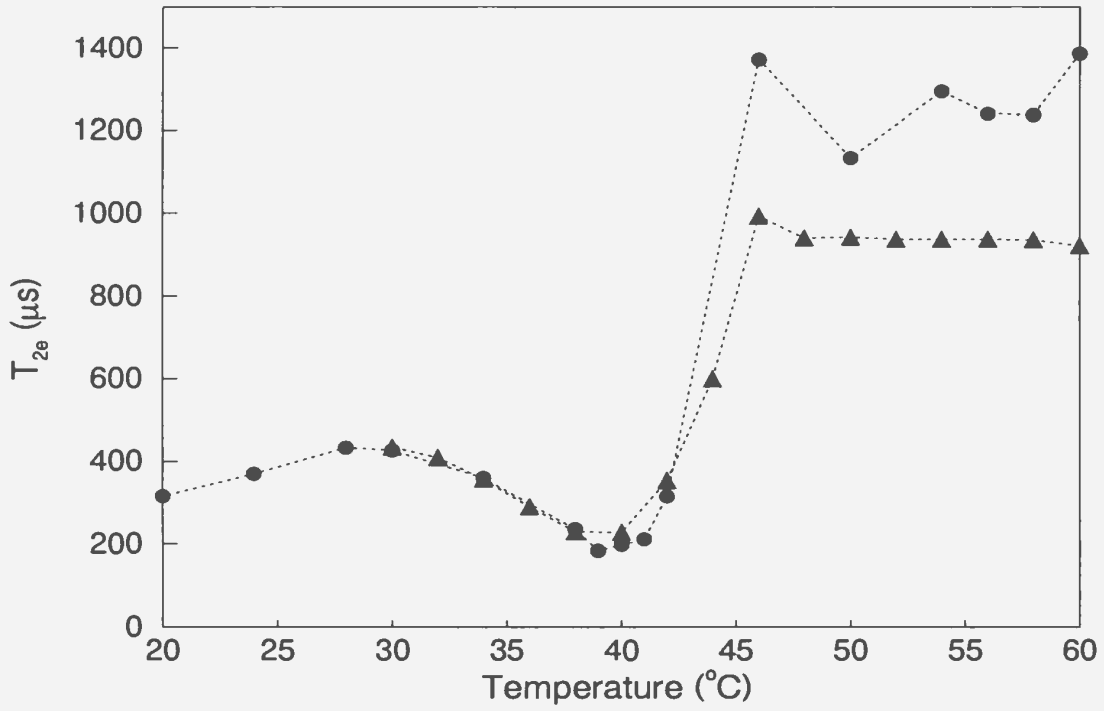

Figure 4.4: T_{2e} relaxation times calculated for the first cooling run (●) of 30% DPPG-d_{62} in DPPC-d_{62} mixed bilayers hydrated in the presence of Ca^{2+}. The sample was subsequently°C warmed back to 64°C and the data represented by (▲) indicates the effect of this second cooling run.

to the method of hydration. Quadrupole echo decays, however, displayed a marked dependence on the hydration protocol. Figure 4.5 shows the temperature dependence of T_{2e} for equimolar mixtures of DPPG-d_{62} in DPPC-d_{62} with Ca^{2+} for different sample histories. By gently stirring the lipids in the buffer it was possible to achieve a state where the hydrated lipids exhibited a high T_{2e} in the liquid crystal phase. Successive heating and cooling cycles irreversibly altered the observed T_{2e} in this phase. During the fourth temperature cycle T_{2e} approaches the behaviour of the corresponding sample prepared by hydrating the lipids in the flask above T_m. This new plateau is observed to be stable for the subsequent cycle. It appears that in these DPPG/DPPC mixtures, the structures formed initially are metastable and evolve towards more stable structures

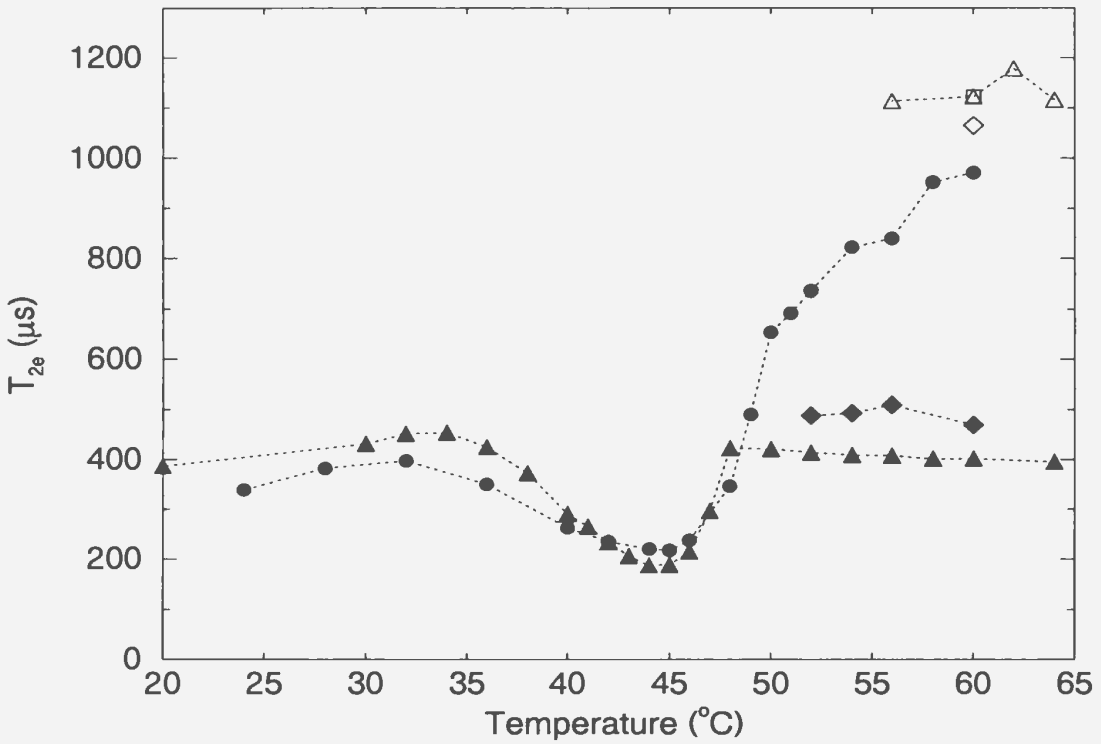

Figure 4.5: T_{2e} times for equimolar DPPG/DPPC bilayers hydrated above T_m (▲) and for first (△), second (□), third (◇), fourth (●) and fifth (◆) heating and cooling cycles for the corresponding sample hydrated with gentle stirring.

with shorter T_{2e} times. Again the T_{2e} behaviour in the gel phase is independent of sample history.

Samples hydrated in the flask above the transition temperature were not observed to evolve with cycling of the temperature. T_{2e} relaxation times are remarkably reproducible for vesicles of 7% DPPG in DPPC prepared with Ca^{2+} buffer in this manner, as shown in figure 4.7. The quadrupolar echo decay is independent of thermal history for this sample. T_{2e} relaxation times of vesicles of 30% DPPG in DPPC prepared using this same hydration protocol are shown in figure 4.8. We observe that Ca^{2+} causes an upward shift of the transition temperature but has negligible effect on T_{2e} in the L_α phase. In the gel phase Ca^{2+} appears to cause the motions dominating the decay rate to freeze out

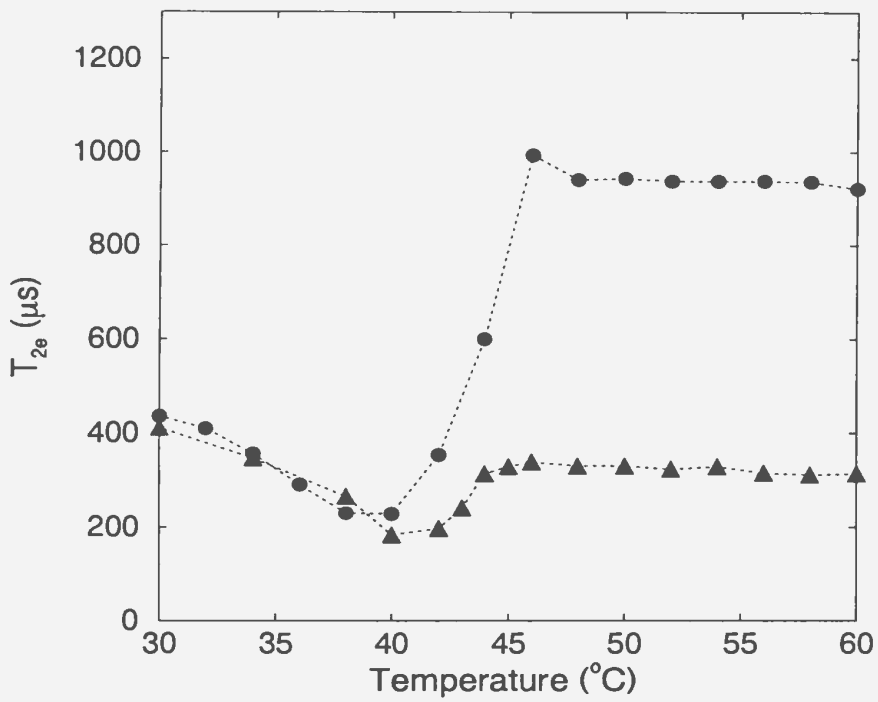

Figure 4.6: T_{2e} times for 30% DPPG in DPPC prepared via gently stirring lipids in buffer (●) and rotating buffer in flask above T_m (▲). Both samples contained Ca^{2+}.

more quickly. Figures 4.7 and 4.8 provide evidence that the ultimate stable structure is insensitive to either Ca^{2+} or to the thermal history of the sample, but is sensitive to the concentration of the anionic component in binary lipid mixtures.

The evolution of T_{2e} towards a lower, stable value indicates that changes induced in the bilayer via temperature cycling are important for the motions which contribute to the decay of the quadrupolar echo in the liquid crystal phase. We have remarked that the first spectral moments for DPPG/DPPC mixed bilayers are insensitive to the thermal history of the sample while T_{2e} evolves with temperature cycling. The order parameters and echo decay times for 30% DPPG in DPPC prepared with Ca^{2+} are presented together for comparison in figure 4.9. While the rates of motions which modulate ω_Q have changed in the L_α region, the average orientation of the acyl chains have not. DPPG and Ca^{2+}

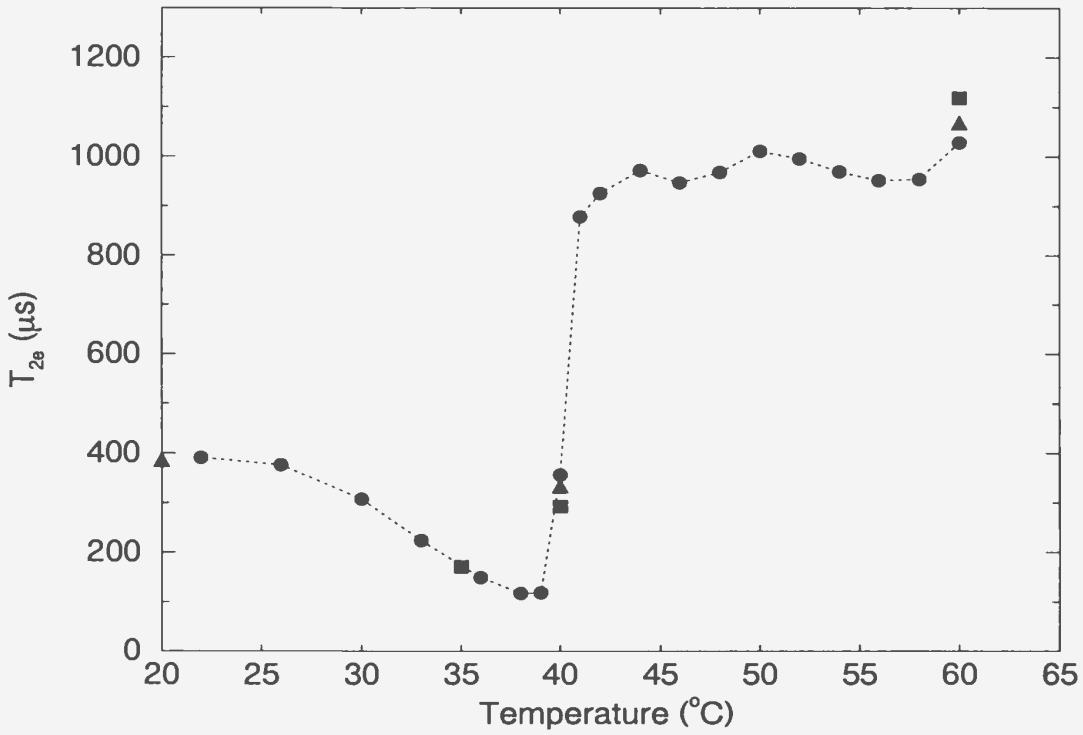

Figure 4.7: T_{2e} times calculated for the first (■), second (▲) and third (●) successive cooling cycles for 7% DPPG-d_{62} in DPPC-d_{62} hydrated by soaking with Ca^{2+} buffer in flask above T_m.

interact with DPPC bilayers in a way which has little effect on the amplitude of the fast chain conformational fluctuations which determine mean orientational order for the perdeuterated chain in the liquid crystalline phase. This is strong evidence that it is the adiabatic motions that have changed since these motions do not contribute to motional narrowing.

In figures 4.10 and 4.11 we observe that for the samples hydrated with gentle stirring, the T_{2e} behaviour evolves with temperature cycling even in the absence of calcium. The effect was considerably more pronounced for equimolar mixtures of DPPC-d_{62} and DPPG-d_{62} than for pure DPPC-d_{62} bilayers. This suggests that the sensitivity to sample preparation is likely associated with DPPG rather than with calcium. The metastable

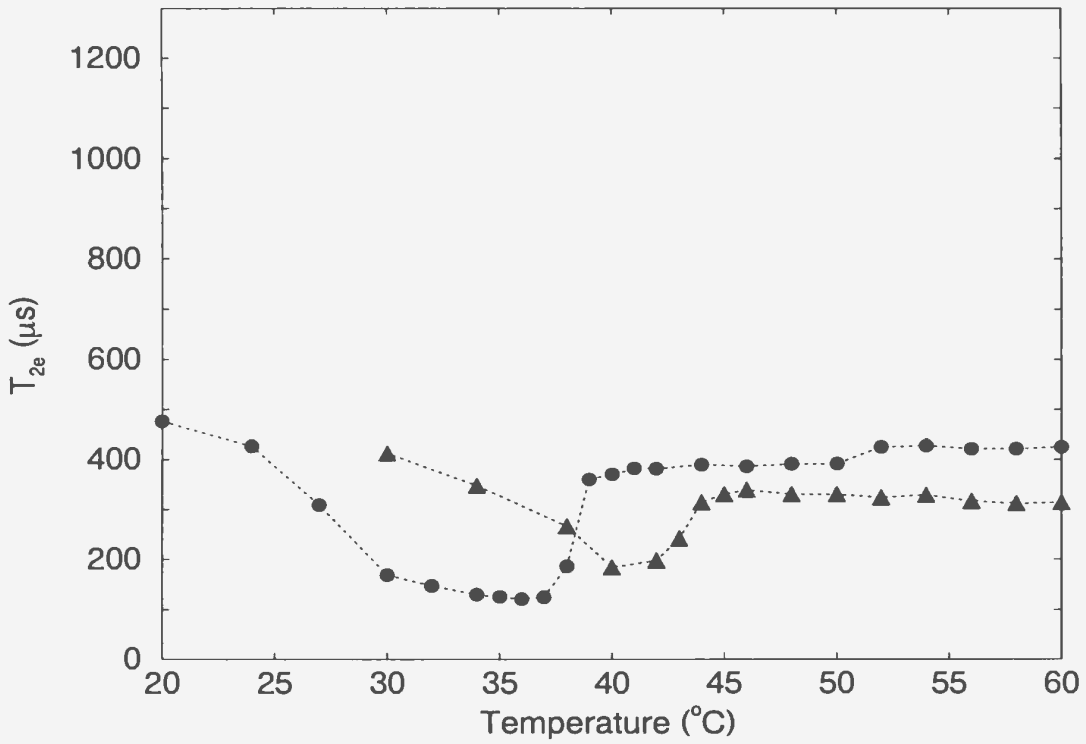

Figure 4.8: T_{2e} temperature profiles for 30% DPPG-d_{62} in DPPC-d_{62} hydrated in a flask above T_m in the absence (▲) and presence (●) of Ca^{2+}.

structures become progressively less stable with respect to their ultimate state as the proportion of DPPG in DPPC increases.

While temperature cycling is observed to significantly alter deuteron transverse relaxation in the liquid crystal phase, the echo decay rate in the gel phase of these bilayer systems is insensitive to successive heating and cooling. This implies that the motions in the liquid crystal regime which are affected by the thermal history of the sample are those which are already on the slow side of the T_{2e} minimum and freeze out at the transition. Those motions which are not frozen out at the transition are apparently not affected by temperature cycling.

By comparing relaxation rates for samples containing 30% DPPG in DPPC with

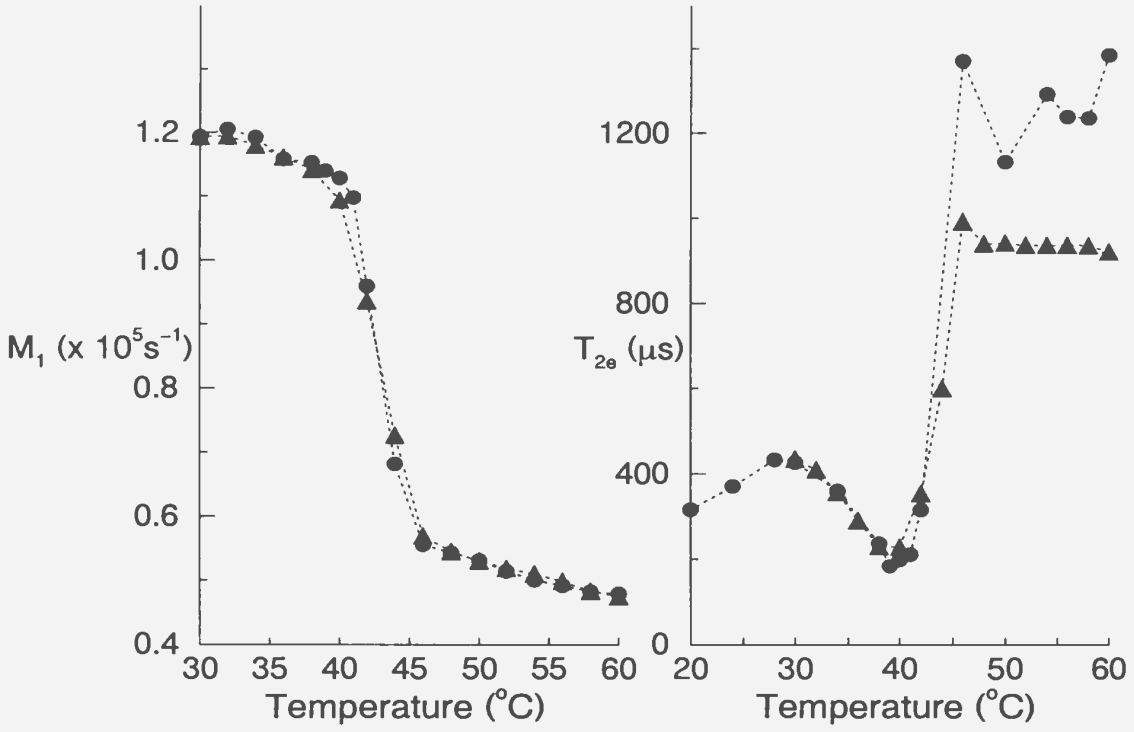

Figure 4.9: M_1 order parameters (left) and T_{2e} relaxation times (right) for the first cooling run (●) of 30% DPPG-d_{62} in DPPC-d_{62} mixed bilayers hydrated in the presence of Ca^{2+}; (▲) indicates the effect the second cooling run.

either one or both lipids deuterated, it is possible to determine whether the motions in DPPG and DPPC acyl chains differ in mixtures of the two lipids in the presence of calcium. From section 3.2 we expect that there will be some isotope effect in the position of the T_{2e} minimum. In figure 4.12 it is seen that the quadrupolar echo decay rates for DPPG/DPPC-d_{62}, DPPG-d_{62}/DPPC and DPPG-d_{62}/DPPC-d_{62} are similar in the gel phase. The difference in the height of the T_{2e} plateau in the liquid crystalline phase for the mixture with both lipids deuterated may be a reflection of the sample preparation and not a real difference in the effectiveness of the motions which dominate T_{2e} in modulating the quadrupolar interaction.

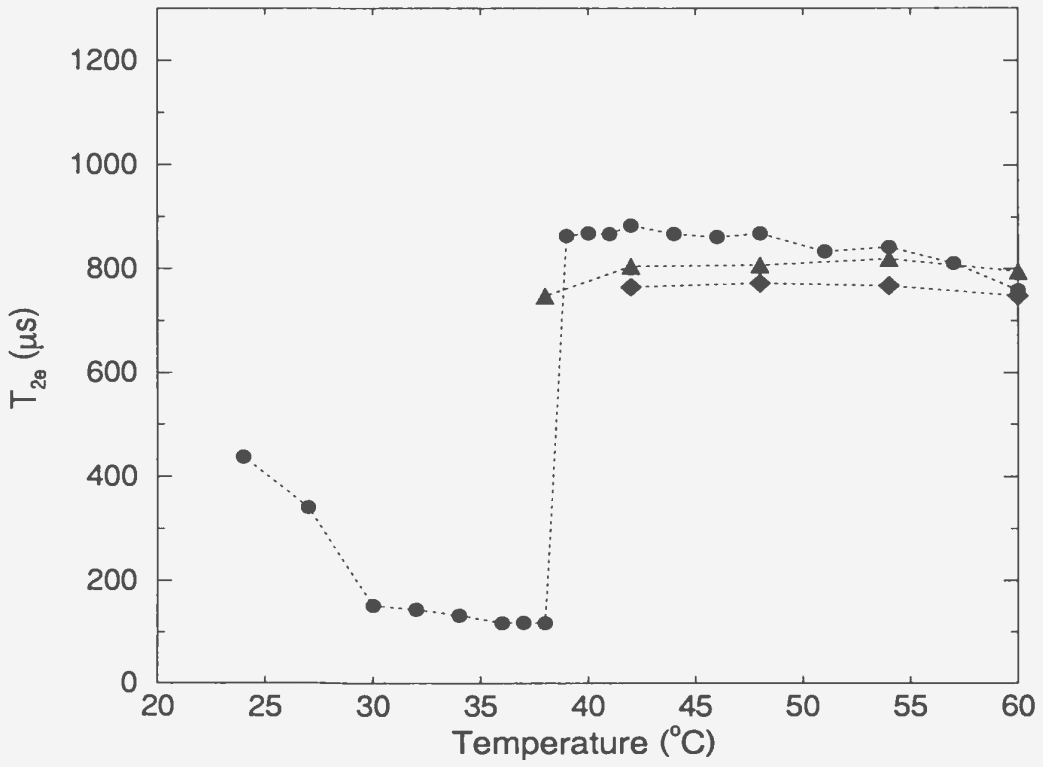

Figure 4.10: T_{2e} times calculated for the first cooling run (●) of pure DPPC-d_{62} hydrated in the absence of Ca^{2+}; (▲) and (◆) indicate the effect of successive cooling cycles.

4.2.1 Summary

In DPPG/DPPC mixtures the behaviour of the quadrupolar echo decay in the liquid crystal phase is curious. With an appropriate choice of hydration protocol it is possible to prepare the multilamellar vesicles in a metastable state with respect to more stable structures to which they eventually transform upon repeated heating and cooling. The formation of this metastable state depends on the DPPG content in the mixtures. This evolution is manifested only in T_{2e} in the liquid crystal phase. McElhaney *et al.* [19] observed changes in lipid packing in the gel phase of pure DPPG upon prolonged incubation at low temperatures. No investigation into the motions in pure DPPG bilayers was performed by these authors.

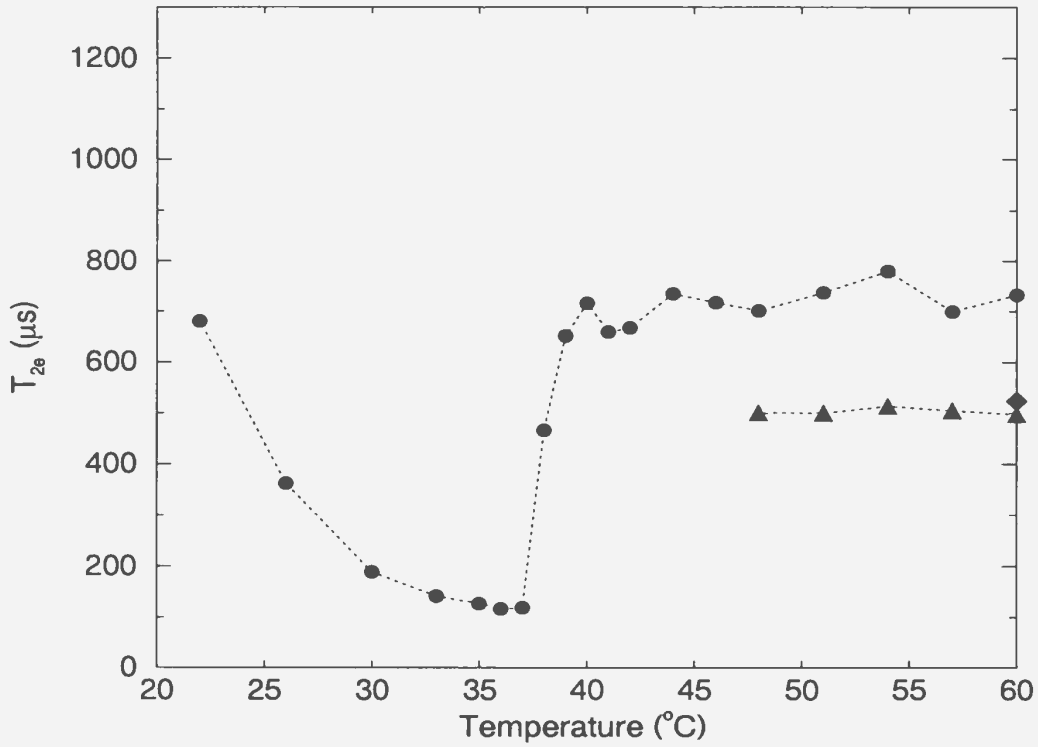

Figure 4.11: T_{2e} times calculated for the first cooling run (●) of equimolar DPPG-d_{62}/DPPC-d_{62} mixed bilayers hydrated in the absence of Ca^{2+}; (▲) and (◆) indicate the effect of successive heating and cooling cycles.

In the ultimate hydration state in our samples the echo decay time in the L_α state is stable and lower when DPPG is present in the mixtures. Calcium does not have a significant effect on T_{2e} when the multilamellar vesicles are in their ultimate stable state. It appears that the sensitivity of the slow motions in the liquid crystal phase to sample preparation is associated with the anionic lipid rather than with calcium. Since the quadrupolar splittings are insensitive to the thermal history of the sample, it is unlikely that ΔM_2 for the faster motions changes as mixtures prepared by gentle stirring in buffer evolve towards their stable states. The reduction in T_{2e} with temperature cycling in these mixtures might be accounted for by a decrease in τ_c for the slow motions, or alternatively by an increase in τ_c for the fast motions in the liquid crystal phase. It is difficult to

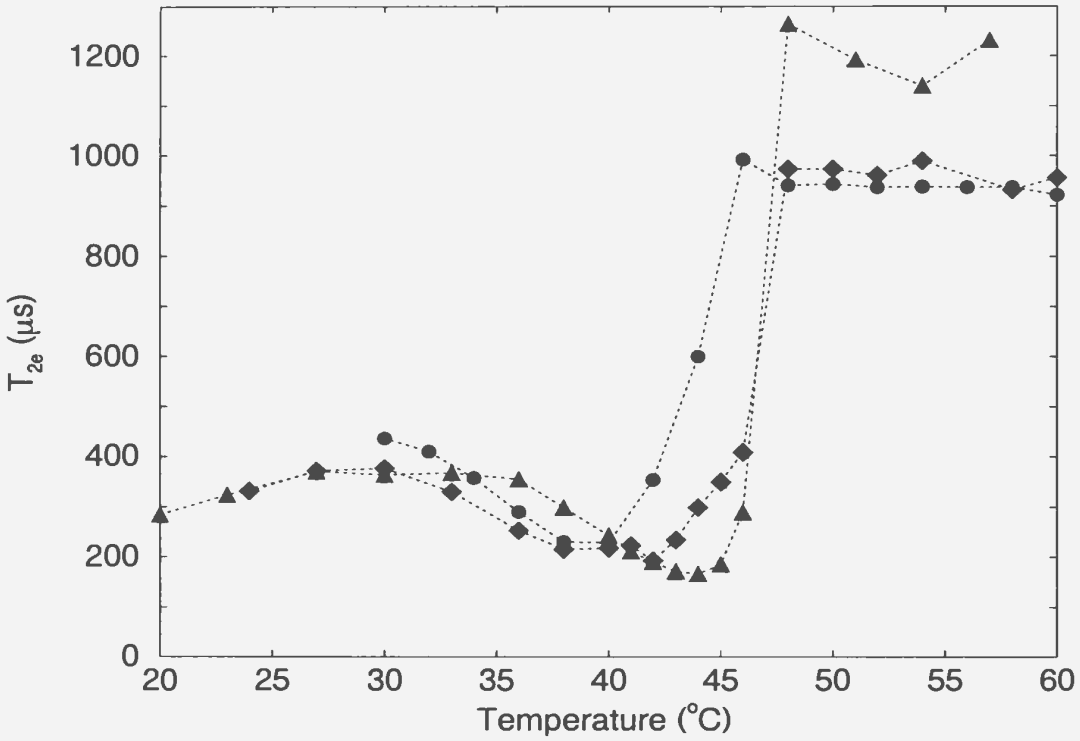

Figure 4.12: Isotopic substitution effects for samples containing 30% DPPG in DPPC with calcium ion present. T_{2e} temperature profiles are shown for DPPG/DPPC-d_{62} (◆), DPPG-d_{62}/DPPC (▲), and DPPG-d_{62}/DPPC-d_{62} (●) mixed bilayers.

conceive that a change tending to decrease the rate of chain isomerisation or rotational diffusion would not result in a change in lateral organisation of the bilayer. On the other hand alterations in the hydrogen bonding network or the hydration layer at the bilayer surface could conceivably occur with repeated heating and cooling cycles, especially if such a network is disrupted by the incorporation of DPPG into the membrane. If T_{2e} is dominated by very slow motions involving large length scales, such as collective motions and diffusion around a vesicle surface, their correlation times could be affected by changes in hydration or order in the headgroup region.

Samples prepared using different hydration protocols may very well have different distributions of vesicle sizes which could determine the dominant relaxation mechanism.

For example, lateral diffusion should contribute more strongly to transverse spin relaxation for smaller vesicles than for larger multilamellar vesicles. It is not clear, however, that temperature cycling should be expected to affect vesicle size in a reproducible way. Importantly, the gel phase behaviour of T_{2e} is insensitive to the hydration protocol. The motions responsible for transverse relaxation in the gel phase are predominantly localised reorientations which might be expected to be less sensitive to the details of vesicle formation or bilayer hydration.

A disruption of the bilayer surface with the incorporation of DPPG is consistent with the results of Kwon *et al.* [23], who observe that DPPG vesicles are more disordered than DPPC vesicles in a recent FTIR study. Their results also suggest that the carbonyl groups in the interfacial region of hydrated phospholipids participate in hydrogen bonding. McElhaney *et al.* argue that DPPG may be able to mimic the behaviour of water molecules for hydration sites in pure DPPG vesicles [19]. If DPPG is competing with water for hydration sites in the DPPG/DPPC mixtures under study, unstable or metastable hydration states could result. More work needs to be done to arrive at a better understanding of the important interactions in DPPG/DPPC mixed bilayers.

5

Concluding Remarks

Deuterium NMR was used to study the order, dynamics and phase behaviour of DPPG/DPPC mixed bilayers in the absence and presence of calcium. By using the available information from ^{2}H NMR spectra we have been able to determine that in the presence of Ca^{2+} the transition temperature and lateral packing density of the acyl chains increase modestly with increasing proportion of the DPPG component in these mixtures. A possible explanation is charge neutralisation and the resulting reduction in electrostatic repulsion between the headgroups, which would be reflected in an increased lateral pressure. However, although there is little doubt that these effects are important, it is difficult to categorically assign the observed effects to the influence of electrostatic headgroup interactions given the differences in phase behaviour of various anionic/zwitterionic mixtures [14] [21] [22].

For systems with quadrupolar interactions, the orientation of the principal axis coordinate system with respect to the magnetic field depends on the molecular motions. The decay of the quadrupolar echo is an excellent indication of the possible motions that may be contributing to relaxation. Our results from quadrupolar echo measurements lead us to conclude that hydration and hydrogen bonding are also important in influencing the

dynamics of these mixed bilayers.

With an appropriate choice of hydration protocol it was possible to prepare the multilamellar vesicles in a metastable state with respect to more stable structures to which they eventually transform upon repeated heating and cooling. During this evolution the echo decay time decreases in the L_α phase when DPPG is present in the mixtures. This can be accounted for by an increase in the rates of slow motions which dominate the echo decay in the liquid crystal phase. The introduction of a negatively charged lipid component into DPPC membranes may alter the hydrogen bonding or modify the water layer at the surface, or both.

If cycling the temperature alters factors such as hydration at the bilayer surface in these mixtures, there does not appear to be any effect on the lateral organisation of the lipids. This leads us to conclude that the motions which are affected by the presence of the anionic lipid are large length scale motions such as diffusion around curved vesicle surfaces or bilayer collective modes. These motions might be expected to be sensitive to such things as hydration and vesicle size. More local motions such as chain libration, lipid rotational diffusion and *trans-gauche* isomerisation were not observed to be sensitive to the concentration of DPPG in the mixed bilayers.

Lung surfactant contains phosphatidylcholine with a large amount of anionic lipid. It is unclear whether the role of anionic lipids in lung surfactant is mediated by the actual chemical nature of the lipids or by an induced condensed state of the lipid domain. The question arises as to whether the role of the anionic lipid in large scale rearrangements in lung surfactant is related to its complicated effects on slow motions observed here.

The extraction of specific correlation times for the motions under discussion requires analysis of the quadrupole echo decays via a detailed model. Such a study is beyond the scope of this thesis but would be a next logical step in interpreting our relaxation data. These results also provide a basis for future studies for modeling the behaviour of DPPG/DPPC mixtures based on hydrogen bonds and hydration forces.

A larger effect on motions and more interesting phase behaviour might be seen in shorter chain systems where the interactions at the bilayer surface might be expected to be greater. Conversely, a smaller effect might be observed in unsaturated chains where the relative roles of headgroups and chains are expected to differ. Other interesting extensions of this study would be to binary lipid systems containing different anionic lipids. Investigators of these systems have tended to focus on the influence of the anionic lipid or divalent cations on ordering of the lipid headgroups and acyl chains. An analysis of the motional behaviour in these systems has not been pursued. The interesting behaviour described here might be expected to be observed to varying degrees in binary systems containing, for example, PS, PA or PI in which the network of hydrogen bonding is thought to be quite different. This would lead to a better understanding of the various interactions at bilayer surfaces and of the nature of hydration forces in general.

Bibliography

[1] M. Bloom, E. Evans, and O. G. Mouritsen. Physical properties of the fluid lipid-bilayer component of cell membranes: a perspective. *Quarterly Reviews of Biophysics*, 24(3), 1991.

[2] F. Brugè, S. L. Fornili, G. G. Malenkov, M. B. Palma-Vittorelli, and M. U. Palma. Solvent-induced forces on a molecular scale: non-additivity, modulation and causal relation to hydration. *Chem. Phys. Lett.*, 254, 1996.

[3] C. Tanford. *The Hydrophobic Effect.* John Wiley and Sons, New York, 1980.

[4] S. Marčelja. Chain ordering in liquid crystals II: Structure of bilayer membranes. *Biochim. Biophys. Acta*, 367:165–176, 1974.

[5] J. N. Israelachvili, S. Marčelja, and R. G. Horn. Physical principles of membrane organization. *Quarterly Reviews of Biophysics*, 13(2):121–200, 1980.

[6] B. Halle. ^{2}H NMR relaxation in phospholipid bilayers. Towards a consistent molecular interpretation. *J. Phys. Chem.*, 95:6724–6733, 1991.

[7] N. Peterson and S. Chan. More on the motional state of lipid bilayer membranes: Interpretation of order parameters obtained from nuclear magnetic resonance. *Biochemistry*, 16(12):2657–2667, 1977.

[8] P. Yeagle. *The Structure of Biological Membranes.* CRC Press, Boca Raton, 1991.

[9] M. Bloom and E. Sternin. Transverse nuclear spin relaxation in phospholipid bilayer membranes. *Biochemistry*, 26:2101–2105, 1987.

[10] J. Stohrer, G. Gröbner, D. Reimer, K. Weisz, C. Mayer, and G. Kothe. Collective lipid motions in bilayer membranes studied by transverse deuteron spin relaxation. *J. Chem. Phys.*, 95(1), 1991.

[11] P. I. Watnick, P. Dea, and S. I. Chan. Characterization of the transverse relaxation rates in lipid bilayers. *Proc. Natl. Acad. Sci. USA*, 87:2082–2086, 1990.

[12] M. Bloom and E. Evans. Observation of surface undulations on the mesoscopic length scale by NMR. In L. Peliti, editor, *Biologically Inspired Physics*, pages 137–147. Plenum Press, New York, 1991.

[13] P. A. Forsythe, S. Marčelja, D. J. Mitchell, and B. W. Ninham. Phase transition in charged lipid membranes. *Biochim. Biophys. Acta*, 469:335–344, 1977.

[14] K. Jacobson and D. Papahadjopoulos. Phase transitions and phase separations in phospholipid membranes induced by changes in temperature, pH, and concentration of bivalent cations. *Biochemistry*, 14(1):152–161, 1975.

[15] Hermann Traüble and H. Eibl. Electrostatic effects on lipid phase transitions: membrane structure and ionic environment. *Proc. Nat. Acad. Sci. USA*, 71(1):214–219, 1974.

[16] F. Borle and J. Seelig. Ca^{2+} binding to phosphatidylglycerol bilayers as studied by differential scanning calorimetry and ^{2}H- and ^{31}P-nuclear magnetic resonance. *Chemistry and Physics of Lipids*, 36:263–283, 1985.

[17] E. G. Finer and A. Darke. Phospholipid hydration studied by deuteron magnetic resonance spectroscopy. *Chem. Phys. Lipids*, 12:1–16, 1974.

[18] G. Cevc and D. Marsh. *Phospholipid Bilayers: Physical Principles and Models.* John Wiley & Sons, New York, 1987.

[19] Y. P. Zhang, R. N. A. H. Lewis, and R. N. McElhaney. Calorimetric and spectroscopic studies of the thermotropic phase behavior of the *n*-saturated 1,2-diacylphosphatidylglycerols. *Biophysical Journal*, 10:779–793, 1997.

[20] E. Findlay and P. Barton. Phase behaviour of synthetic phosphatidylglycerols and binary mixtures with phosphatidylcholines in the presence and absence of calcium ions. *Biochemistry*, 17(12):2400–2404, 1978.

[21] P. W. M. van Dijck, B. de Kruijff, A. J. Verkleij, L. L. M. van Deenen, and J. de Gier. Comparative studies on the effects of pH and Ca^{2+} on bilayers of various negatively charged phospholipids and their mixtures with phosphatidylcholine. *Biochim. Biophys. Acta*, 512:84–96, 1978.

[22] A. G. Lee. Lipid phase transitions and mixtures. In Roland C. Aloia, editor, *Membrane Fluidity in Biology, Vol. 2*, chapter 3. Academic Press, Inc., New York, 1983.

[23] K. O. Kwon, M. J. Kim, M. Abe, T. Ishinomori, and K. Ogino. Thermotropic behaviour of a phospholipid bilayer interacting with metal ions. *Langmuir*, 10:1415–1420, 1994.

[24] A. S. Dico, J. Hancock, M. R. Morrow, J. Stewart, S. Harris, and K. M. W. Keough. Pulmonary surfactant protein SP-B interacts similarly with dipalmitoylphosphatidylglycerol and dipalmitoylphosphatidylcholine in phosphatidylcholine/phosphatidylglycerol mixtures. *Biochemistry*, 36(14):4172–4177, 1997.

[25] A. S. Dico, J. Hancock, M. R. Morrow, and K. M. W. Keough. Effect of calcium on phospholipid interaction with pulmonary surfactant C. 1997. *Submitted to Biophysical Journal.*

[26] T. J. Pinheiro and A. Watts. Lipid specificity in the interaction of cytochrome c with anionic phospholipid bilayers revealed by solid-state ^{31}P-NMR. *Biochemistry*, 30:2451–2458, 1994.

[27] H. H. de Jongh, T. Ritsema, and J. A. Killian. Lipid specificity for membrane mediated partial unfolding of cytochrome c. *FEBS Lett.*, 360:255–260, 1995.

[28] W. Xia and W. Dowhan. In vivo evidence for the involvement of anionic phospholipids in initiation of DNA replication in *Escherichia coli. Proc. Natl. Acad. Sci. USA*, 92:783–787, 1995.

[29] F. Sixl and A. Watts. Headgroup interactions in mixed phospholipid bilayers. *Proc. Natl. Acad. Sci.*, 80:1613, 1983.

[30] R. Zidovetski, A. Atiya, and H. de Boeck. Effect of divalent cations on the structure of dipalmitoylphosphatidylcholine and phosphatidylcholine/phosphatidylglycerol bilayers: An ^{2}H-NMR study. *Membrane Biochemistry*, 8:177–186, 1989.

[31] J. H. Davis. The description of lipid conformation, order, and dynamics by ^{2}H NMR. *Biochim. Biophys. Acta*, 737:117–171, 1983.

[32] D. I. Hoult. The NMR receiver: A description and analysis of design. *Progress in NMR Spectroscopy*, 12:44–77, 1978.

[33] G. J. Bowden and W. D. Hutchison. Tensor operator formalism for multiple-quantum NMR. 1. Spin-1 nuclei. *Journal of Magnetic Resonance*, 67:403–414, 1986.

[34] M. Mehring. *Principles of High-Resolution NMR in Solids.* Springer-Verlag, Berlin, 2nd edition, 1983.

[35] C. P. Slichter. *Principles of Magnetic Resonance.* Springer-Verlag, Heidelberg, 1990.

[36] H. W. Spiess. In P. Diehl, E. Fluck, H. Gunther, R. Kosfeld, and J. Seelig, editors, *NMR: Basic Principles and Progress, Vol. 15.* Springer-Verlag, Berlin, 1978.

[37] J. H. Davis. Deuterium nulear magnetic resonance spectroscopy in partially ordered systems. In E. Buncel and J.R. Jones, editors, *Isotopes in the Physical and Biomedical Sciences, Vol. 2*, chapter 3. Elsevier Science Publishers, Amsterdam, 1991.

[38] E. Fukushima and S. Roeder. *Experimental Pulse NMR: A Nuts and Bolts Approach.* Addison-Wesley, London, 1981.

[39] J. Seelig. Deuterium magnetic resonance; theory and application to lipid membranes. *Quarterly Reviews of Biophysics*, 10:353–418, 1977.

[40] A. Abragam. *The Principles of Nuclear Magnetism.* Clarendon Press, Oxford, 1961.

[41] R. R. Ernst, G. Bodenhausen, and A. Wokaun. *Principles of Nuclear Magnetic Resonance in One and Two Dimensions.* The International Series of Monographs on Chemistry. Oxford University Press, Oxford, 1987.

[42] M. Bloom. NMR studies of membranes and whole cells. In *Enrico Fermi International School on the Physics of Magnetic Resonance in Medicine*, The Netherlands, 1987. Societá Italiana di Fisica, Elsevier Science Publishers.

[43] J. H. Davis, K. R. Jeffrey, M. Bloom, M. I. Valic, and T. P. Higgs. Quadrupolar echo deuteron magnetic resonance spectroscopy in ordered hydrocarbon chains. *Chem. Phys. Lett.*, 42:390–394, 1976.

[44] N. Bloembergen, E. M. Purcell, and R. V. Pound. Relaxation effects in nuclear magnetic resonance absorption. *Phys. Rev.*, 73:679–712, 1948.

[45] M. Bloom, E.E. Burnell, A. L. MacKay, C. P. Nichol, M. I. Valic, and G. Weeks. Fatty acyl chain order in lecithin model membranes determined from proton magnetic resonance. *Biochemistry*, 17(26):5750–5762, 1978.

[46] K. P. Pauls, A. L. MacKay, O. Söderman, M. Bloom, A. K. Tanjea, and R. S. Hodges. Dynamic properties of the backbone of an integral membrane polypeptide measured by ^{2}H-NMR. *European Biophysics Journal*, 12:1–11, 1985.

[47] M. Bloom, J. H. Davis, and A. L. MacKay. Direct determination of the oriented sample NMR spectrum from the powder spectrum for systems with local axial symmetry. *Chem. Phys. Lett.*, 80:198–202, 1981.

[48] E. Sternin, M. Bloom, and A. L. MacKay. De-Pake-ing of NMR spectra. *Journal of Magnetic Resonance*, 55:274–282, 1983.

[49] S. Prosser and J. H. Davis. Deuterium NMR relaxation studies of peptide-lipid interactions. *Biochemistry*, 31(39):9355–9363, 1992.

[50] R. G. Griffin. Solid state nuclear magnetic resonance in lipid bilayers. *Methods Enzym.*, 72:108–174, 1981.

[51] M. R. Morrow, J. C. Huschilt, and J. H. Davis. Simultaneous modeling of phase and calorimetric behaviour in an amphiphilic peptide/phospholipid model membrane. *Biochemistry*, 24(20):5396–5406, 1985.

[52] J. C. Huschilt, R. S. Hodges, and J. H. Davis. Phase equilibria in an amphiphilic peptide-phospholipid model membrane by deuterium nuclear magnetic resonance difference spectroscopy. *Biochemistry*, 24(6):1377–1386, 1985.

[53] C. Altenbach and J. Seelig. Ca^{2+} binding to phosphatidylcholine bilayers as studied by deuterium magnetic resonance. Evidence for the formation of a Ca^{2+} complex with two phospholipid molecules. *Biochemistry*, 23(17):3913–3920, 1984.

[54] J. H. Davis. Deuterium magnetic resonance study of the gel and liquid crystalline phases of dipalmitoyl phosphatidylcholine. *Biophysical Journal*, 27:339–358, 1992.

[55] M. F. Brown and O. Söderman. Orientational anisotropy of nuclear spin relaxation in phospholipid membranes. *Chem. Phys. Lett.*, 167, 1990.

[56] C. Morrison. Theory of the general orientation dependence of ^{2}H NMR spin-lattice relaxation and experiments on model membranes. Master's thesis, University of British Columbia, 1987.

Appendix A

Density Matrix Treatment of Spin 1 Dynamics

The following is a practical application of the more abstract NMR theory of chapter 2. The product operator formalism is used to follow the role of the rf pulses and the quadrupolar interaction during the quadrupolar echo pulse sequence. The commutators for the spin 1 basis operators are tabulated below for convenience (table A.1).

Table A.1: Commutators of spin 1 basis operators.

$\overline{p}$ \ $\overline{q}$	$\overline{1}$	$\overline{2}$	$\overline{3}$	$\overline{4}$	$\overline{5}$	$\overline{6}$	$\overline{7}$	$\overline{8}$
$\overline{1}$	0	$\overline{3}$	$-\overline{2}$	$-\sqrt{3}\,\overline{6}$	$-\overline{8}$	$\sqrt{3}\,\overline{4}+\overline{7}$	$-\overline{6}$	$\overline{5}$
$\overline{2}$	$-\overline{3}$	0	$\overline{1}$	$\sqrt{3}\,\overline{5}$	$-\sqrt{3}\,\overline{4}+\overline{7}$	$\overline{8}$	$-\overline{5}$	$\overline{6}$
$\overline{3}$	$\overline{2}$	$-\overline{1}$	0	0	$\overline{6}$	$-\overline{5}$	$2\overline{8}$	$-2\,\overline{7}$
$\overline{4}$	$\sqrt{3}\,\overline{6}$	$-\sqrt{3}\,\overline{5}$	0	0	$\sqrt{3}\,\overline{2}$	$-\sqrt{3}\,\overline{1}$	0	0
$\overline{5}$	$\overline{8}$	$\sqrt{3}\,\overline{4}-\overline{7}$	$-\overline{6}$	$-\sqrt{3}\,\overline{2}$	0	$\overline{3}$	$\overline{2}$	$-\overline{1}$
$\overline{6}$	$-\sqrt{3}\,\overline{4}-\overline{7}$	$-\overline{8}$	$\overline{5}$	$\sqrt{3}\,\overline{1}$	$-\overline{3}$	0	$\overline{1}$	$\overline{2}$
$\overline{7}$	$\overline{6}$	$\overline{5}$	$-2\,\overline{8}$	0	$-\overline{2}$	$-\overline{1}$	0	$2\overline{3}$
$\overline{8}$	$-\overline{5}$	$\overline{6}$	$2\overline{7}$	0	$\overline{1}$	$-\overline{2}$	$2\overline{3}$	0

*All values in table must be multiplied by $i/\sqrt{2}$.

For deuterium in high fields the quadrupolar interaction is a small perturbation on the Zeeman interaction and $Q_0 \ll I_0$. Therefore we will follow only the evolution and transformation of the Zeeman polarisation I_0 during the experiment. The equilibrium density operator can be expressed in terms of the Cartesian I_z spin operator. Initially, then,

$$\rho(0) = c_3(0)\overline{\mathbf{3}} = -\sqrt{2}\,\hbar\omega_0\overline{\mathbf{3}}.$$

For the first pulse along the y-axis the system evolves under $\mathcal{H}_y = -\sqrt{2}\hbar\omega_1\overline{\mathbf{2}}$ and

$$\left[\mathcal{H}_y, \overline{\mathbf{3}}\right] = -\sqrt{2}\,\hbar\omega_1 \left[\overline{\mathbf{2}}, \overline{\mathbf{3}}\right] = -i\hbar\omega_1\overline{\mathbf{1}}. \tag{A.1}$$

The equation of motion 2.15 for $c_3(t)$ is

$$\begin{aligned} \frac{dc_3(t)}{dt} &= \frac{i}{\hbar}\sum_q c_q(t)\,Tr\left\{P_q\,\left[\mathcal{H}_y, \overline{\mathbf{3}}\right]\right\} \\ &= \omega_1 \sum_q c_q(t)\,Tr\left\{P_q\,\overline{\mathbf{1}}\right\} \\ &= \omega_1 c_1(t). \end{aligned} \tag{A.2}$$

Similarly the equation of motion for $c_1(t)$ is

$$\frac{dc_1(t)}{dt} = -\omega_1 c_3(t). \tag{A.3}$$

The solutions to these two coupled differential equations are

$$\begin{cases} c_1(t_y) &= -I_0 \sin(\omega_1 t_y) \\ c_3(t_y) &= I_0 \cos(\omega_1 t_y). \end{cases} \tag{A.4}$$

Thus I_z precesses into I_x, or in operator space, precession occurs in the $\left(\overline{\mathbf{1}}, \overline{\mathbf{3}}\right)$ plane. For a pulse such that $\omega_1 t_y = \pi/2$, $c_3(t_y) = 0$ and $c_1(t_y) = -I_0$. All of the magnetisation initially aligned along z has precessed into the negative x axis.

Between rf pulses the system evolves subject only to $\mathcal{H}_Q = \sqrt{\frac{2}{3}}\hbar\omega_Q\,\overline{\mathbf{4}}$:

$$\frac{dc_1(t)}{dt} = \frac{i}{\hbar}\sum_q c_q(t)\,Tr\left\{P_q\,\left[\mathcal{H}_Q, \overline{\mathbf{1}}\right]\right\} \tag{A.5}$$

and

$$\left[\mathcal{H}_Q, \overline{\mathbf{1}}\right] = \sqrt{\frac{2}{3}}\,\hbar\omega_Q\,\left[\overline{\mathbf{4}}, \overline{\mathbf{1}}\right] = i\hbar\omega_Q\overline{\mathbf{6}}. \tag{A.6}$$

The quadrupolar Hamiltonian couples $\overline{\mathbf{1}}$ to $\overline{\mathbf{6}}$, so we also need

$$\left[\mathcal{H}_Q, \overline{\mathbf{6}}\right] = \sqrt{\frac{2}{3}}\,\hbar\omega_Q\,\left[\overline{\mathbf{4}}, \overline{\mathbf{6}}\right] = -i\hbar\omega_Q\overline{\mathbf{1}}. \tag{A.7}$$

Precession under the influence of $\mathcal{H}_Q$ is in the $\left(\overline{\mathbf{1}}, \overline{\mathbf{6}}\right)$ plane of Liouville space. In spin space the Quadrupolar Hamiltonian converts the I_x operator into a linear combination of I_yI_z and I_zI_y. Again the evolution is described by two coupled differential equations

$$\frac{dc_1(t)}{dt} = -\omega_Q c_6(t) \quad \text{and} \quad \frac{dc_6(t)}{dt} = \omega_Q c_1(t)$$

whose solutions are

$$\begin{cases} c_1(\tau) &= I_0\cos\left(\omega_Q\tau\right)\,\sin\left(\omega_1 t_y\right) \\ c_6(\tau) &= I_0\sin\left(\omega_Q\tau\right)\,\sin\left(\omega_1 t_y\right). \end{cases} \tag{A.8}$$

When a second pulse is applied along the x axis at $t = \tau$, both $c_1(\tau)$ and $c_6(\tau)$ are non-zero and $\mathcal{H}_x = -\sqrt{2}\hbar\omega_1\overline{\mathbf{1}}$. The equation of motion for $c_1(t)$ is

$$\frac{dc_1(t)}{dt} = \frac{i}{\hbar}\sum_q c_q(t)\,Tr\left\{P_q\,\left[\mathcal{H}_x, \overline{\mathbf{1}}\right]\right\} = 0. \tag{A.9}$$

$c_1(t)$ is thus invariant under this rf pulse. $c_6(t)$ is not invariant since $\mathcal{H}_x$ and $\overline{\mathbf{6}}$ do not commute:

$$\left[\mathcal{H}_x, \overline{\mathbf{6}}\right] = -\sqrt{2}\hbar\omega_1\left[\overline{\mathbf{1}}, \overline{\mathbf{6}}\right] = -2i\hbar\omega_1\frac{1}{2}\left(\sqrt{3}\,\overline{\mathbf{4}} + \overline{\mathbf{7}}\right) \tag{A.10}$$

and

$$\frac{dc_6(t)}{dt} = \frac{i}{\hbar}\sum_q c_q(t)\,Tr\left\{P_q\,\left[\mathcal{H}_x, \overline{\mathbf{6}}\right]\right\} = 2\omega_1\frac{1}{2}\left(\sqrt{3}c_4(t) + c_7(t)\right). \tag{A.11}$$

This suggests that we should also seek

$$\left[\mathcal{H}_x, \frac{1}{2}\left(\sqrt{3}\,\overline{\mathbf{4}} + \overline{\mathbf{7}}\right)\right] = -\frac{1}{\sqrt{2}}\hbar\omega_1\left\{\sqrt{3}\left[\overline{\mathbf{1}}, \overline{\mathbf{4}}\right] + \left[\overline{\mathbf{1}}, \overline{\mathbf{7}}\right]\right\} = 2i\hbar\omega_1\overline{\mathbf{6}} \tag{A.12}$$

and

$$\frac{d}{dt}\left[\frac{1}{2}\left(\sqrt{3}c_4(t) + c_7(t)\right)\right] = \frac{i}{\hbar}\sum_q c_q(t)\,Tr\left\{P_q\,\left[\mathcal{H}_x, \frac{1}{2}\left(\sqrt{3}\,\overline{\mathbf{4}} + \overline{\mathbf{7}}\right)\right]\right\} = -2\omega_1 c_6(t). \tag{A.13}$$

Once again we have two coupled differential equations. Just before the second pulse is applied, $c_4(\tau) = c_7(\tau) = 0$. Then, solutions for pulse length t_x are

$$\begin{cases} c_1(t_x) = \text{invariant} \\ c_6(t_x) = I_0\cos\left(2\omega_1 t_x\right)\sin\left(\omega_Q\tau\right)\sin\left(\omega_1 t_y\right) \\ \frac{1}{2}\left(\sqrt{3}c_4(t_x) + c_7(t_x)\right) = -I_0\sin\left(2\omega_1 t_x\right)\sin\left(\omega_Q\tau\right)\sin\left(\omega_1 t_y\right) \end{cases} \tag{A.14}$$

If both pulses are of duration $\omega_1 t = \pi/2$, then

$$\sqrt{3}c_4(t_x) + c_7(t_x) = 0 \quad \text{and} \quad c_6\left(\tau\right) = -I_0\sin\left(\omega_Q\tau\right).$$

After this second pulse the system is again allowed to evolve under the quadrupolar Hamiltonian. Only $c_1(t)$ and $c_6(t)$ are non-zero and need be examined. The commutators of interest are $\left[\mathcal{H}_Q, \overline{\mathbf{1}}\right]$ and $\left[\mathcal{H}_Q, \overline{\mathbf{6}}\right]$ as obtained above in A.6 and A.7. Again $\mathcal{H}_Q$ couples $\overline{\mathbf{1}}$ to $\overline{\mathbf{6}}$, but with different initial conditions following the two $\pi/2$ pulses:

$$c_1(\tau + t_x) = I_0\cos\left(\omega_Q\tau\right) \quad \text{and} \quad c_6(\tau + t_x) = -I_0\sin\left(\omega_Q\tau\right).$$

Finally, at time t' from the removal of the second pulse,

$$\begin{cases} c_1(t) &= I_0 \left\{ \sin(\omega_Q \tau) \sin(\omega_Q t') + \cos(\omega_Q \tau) \cos(\omega_Q t') \right\} \\ c_6(t) &= I_0 \left\{ \sin(\omega_Q \tau) \cos(\omega_Q t') - \cos(\omega_Q \tau) \sin(\omega_Q t') \right\} . \end{cases} \tag{A.15}$$

From the origin of the pulse sequence $t = t' + \tau$, neglecting t_x and t_y, and the above equations A.15 become

$$\begin{cases} c_1(t) &= I_0 \cos \omega_Q (t - 2\tau) \\ c_6(t) &= -I_0 \sin \omega_Q (t - 2\tau) . \end{cases} \tag{A.16}$$

The trace of $I_x(t)$ provides the expression for the observed NMR signal. The free induction decay (FID) following the first pulse

$$\langle I_x(t) \rangle = \sqrt{2}\, Tr \left\{ \overline{\mathbf{1}} \rho(t) \right\} = \sqrt{2} c_1(t) = \sqrt{2}\, I_0 \cos(\omega_Q t) \tag{A.17}$$

is the Fourier transform of the lineshape of the spin system [42]. Following the second pulse the signal forms an echo at $t = 2\tau$ and then exactly reproduces the FID following the first pulse;

$$\langle I_x(t) \rangle = \sqrt{2}\, Tr \left\{ \overline{\mathbf{1}} \rho(t) \right\} = \sqrt{2} c_1(t) = \sqrt{2}\, I_0 \cos(\omega_Q [t - 2\tau]) . \tag{A.18}$$

Refocussing of the phase memory lost during quadrupolar interactions is complete insofar as relaxation effects have been ignored. Thus the origin of the time domain may be shifted to the peak of the echo without losing any information. A more subtle consequence of this is that the QE signal decays only as a result of randomly fluctuating interactions and not due to any static distribution of quadrupolar splittings [1]. The

Table A.2: Quadrupolar Hamiltonian relaxation rates.

Operator	Relaxation Rate, $A = \frac{4\pi}{5}\omega_Q^2$
$\overline{\mathbf{1}} = \frac{I_x}{\sqrt{2}}, \overline{\mathbf{2}} = \frac{I_y}{\sqrt{2}}$	$\frac{1}{T_2} = A\left[J_0(0) + \frac{5}{3}J_1(\omega_0) + \frac{2}{3}J_2(2\omega_0)\right]$
$\overline{\mathbf{3}} = \frac{I_z}{\sqrt{2}}$	$\frac{1}{T_{1Z}} = A\frac{2}{3}\left[J_1(\omega_0) + 4J_2(2\omega_0)\right]$
$\overline{\mathbf{4}} = \frac{1}{\sqrt{6}}\left(3I_z^2 - 2\right)$	$\frac{1}{T_{1q}} = 2AJ_1(\omega_0)$
$\overline{\mathbf{5}} = \frac{1}{\sqrt{2}}\left(I_xI_z + I_zI_x\right), \overline{\mathbf{6}} = \frac{1}{\sqrt{2}}\left(I_yI_z + I_zI_y\right)$	$\frac{1}{T_{2q}} = A\left[J_0(0) + \frac{1}{3}J_1(\omega_0) + \frac{2}{3}J_2(2\omega_0)\right]$
$\overline{\mathbf{7}} = \frac{1}{\sqrt{2}}\left(I_x^2 - I_y^2\right), \overline{\mathbf{8}} = \frac{1}{\sqrt{2}}\left(I_xI_y + I_yI_x\right)$	$\frac{1}{T_{DQ}} = 2A\left[J_1(\omega_0) + 2J_2(2\omega_0)\right]$

quadrupolar relaxation rates in terms of the spectral densities $J_0(0)$, $J_1(\omega_0)$ and $J_2(2\omega_0)$ for the spin 1 basis operators are provided in table A.2 [56].

$\mathcal{H}_z = -\sqrt{2}\omega_o \bar{3}$

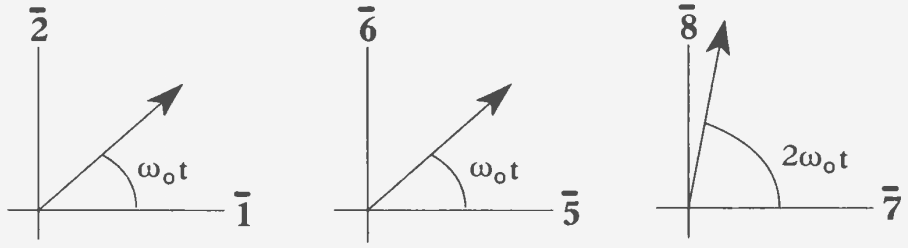

Invariants: $\bar{3}, \bar{4}$

$\mathcal{H}_Q = \sqrt{\frac{2}{3}}\,\omega_Q \bar{4}$

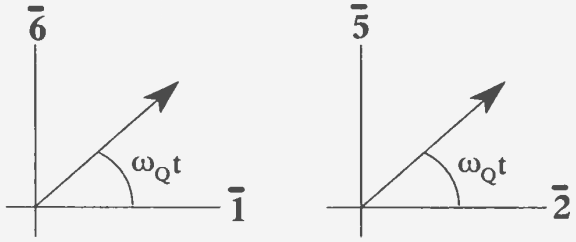

Invariants: $\bar{3}, \bar{4}, \bar{7}, \bar{8}$

$\mathcal{H}_x = -\sqrt{2}\omega_1 \bar{1}$

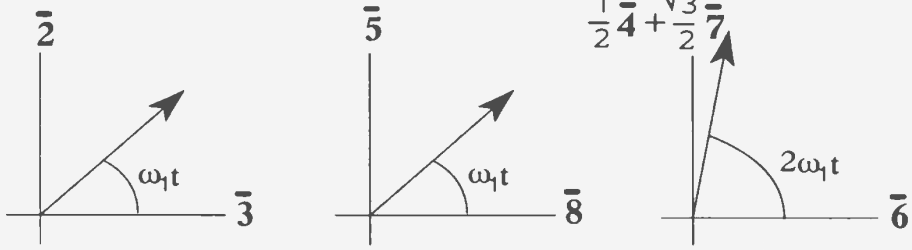

Invariants: $\bar{1}, \frac{1}{2}\bar{4} - \frac{\sqrt{3}}{2}\bar{7}$

$\mathcal{H}_y = -\sqrt{2}\omega_1 \bar{2}$

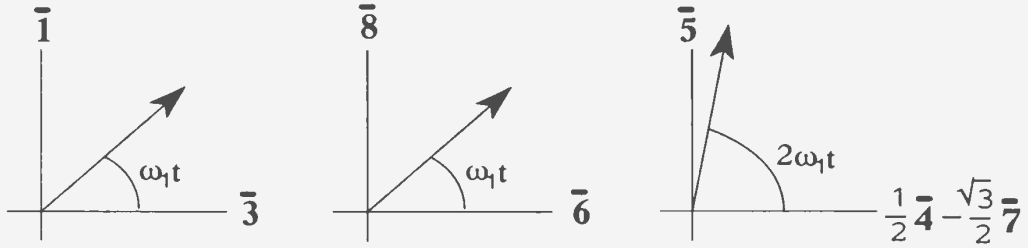

Invariants: $\bar{2}, \frac{1}{2}\bar{4} + \frac{\sqrt{3}}{2}\bar{7}$

Appendix B

Wigner Rotation Matrices

Radiofrequency pulses applied down a specific axis induce rotations in a plane orthogonal to that axis. To describe a rotation about an arbitrary axis, we use the Euler angles. In general this involves three successive rotations,

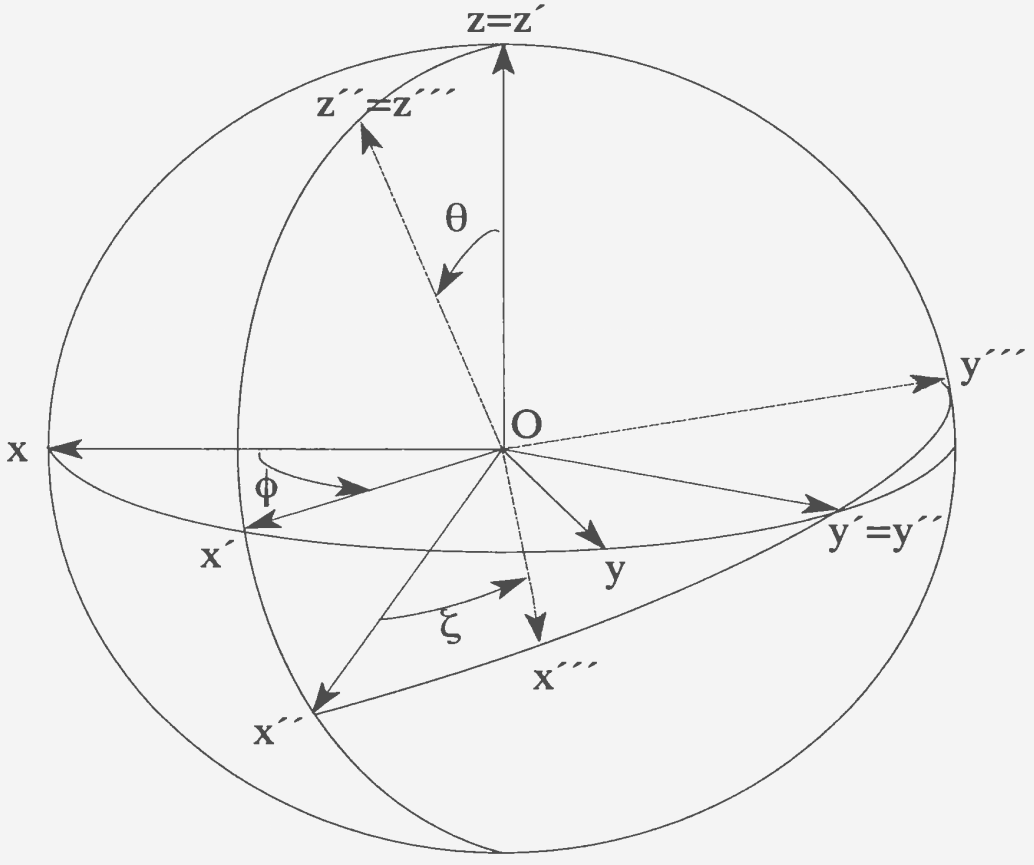

Figure B.1: The Eulerian angles ϕ, θ, ξ defined for right-handed rotations.

- α about the z axis

- β about the new y axis - y'
- γ about the resulting z axis - z''.

The general rotation operator is written

$$\mathbf{D}(\alpha\,\beta\,\gamma) = e^{-i\gamma I_z''}\, e^{-i\beta I_y'}\, e^{-i\alpha I_z};$$

alternatively, we can define the rotations with respect to the original axes:

$$\mathbf{D}(\alpha\,\beta\,\gamma) = e^{-i\alpha I_z}\, e^{-i\beta I_y}\, e^{-i\gamma I_z}.$$

The Wigner rotation matrix is defined as

$$\mathbf{D}(\alpha\,\beta\,\gamma) = \left\langle m|e^{-i\alpha I_z}\, e^{-i\beta I_y}\, e^{-i\gamma I_z}|m'\right\rangle,$$

as shown in figure B.1. $|m\rangle$ and $|m'\rangle$ are eigenstates for spin I and in a basis where I_z is diagonal i.e.

$$I_z|m\rangle = m|m\rangle.$$

For these states,

$$\mathrm{D}^k_{mm'}(\alpha\,\beta\,\gamma) = e^{-i\alpha m}\, d^k_{mm'}(\beta)\, e^{-i\gamma m'}$$

where k is the rank of the tensor and

$$d^k_{mm'}(\beta) = \left\langle m|e^{-i\beta I_y}|m'\right\rangle$$

is the reduced rotation matrix. Values for elements of $d^k_{mm'}(\beta)$ are tabulated elsewhere [34].

As an example, for $I = 1$, $m, m' = \{1, 0, -1\}$

$$d^1(\beta) = \begin{pmatrix} \frac{1}{2}(1+\cos\beta) & -\frac{1}{\sqrt{2}}\sin\beta & \frac{1}{2}(1-\cos\beta) \\ \frac{1}{\sqrt{2}}\sin\beta & \cos\beta & -\frac{1}{\sqrt{2}}\sin\beta \\ \frac{1}{2}(1-\cos\beta) & \frac{1}{\sqrt{2}}\sin\beta & \frac{1}{2}(1+\cos\beta) \end{pmatrix}$$

and

$$\mathrm{D}^1(\alpha, \beta, -\alpha) = \begin{bmatrix} \delta & -\xi & \zeta \\ \xi^\dagger & \varepsilon & -\xi \\ \zeta^\dagger & \xi^\dagger & \delta \end{bmatrix}$$

where

$$\begin{aligned} \delta &= \cos^2(\beta/2) \\ \xi &= \sqrt{2}\cos(\beta/2)\sin(\beta/2)\, e^{-i\alpha} \\ \zeta &= \sin^2(\beta/2)\, e^{-2i\alpha} \\ \varepsilon &= \cos^2(\beta/2) - \sin^2(\beta/2) = \cos\beta \end{aligned}$$

$$\mathrm{D}^1 \quad (\alpha, \beta, -\alpha)$$

$$= \begin{bmatrix} \cos^2(\beta/2) & -\sqrt{2}\cos(\beta/2)\sin(\beta/2)\, e^{-i\alpha} & \sin^2(\beta/2)\, e^{-2i\alpha} \\ \sqrt{2}\cos(\beta/2)\sin(\beta/2)\, e^{i\alpha} & \cos\beta & -\sqrt{2}\cos(\beta/2)\sin(\beta/2)\, e^{-i\alpha} \\ \sin^2(\beta/2)\, e^{2i\alpha} & \sqrt{2}\cos(\beta/2)\sin(\beta/2)\, e^{i\alpha} & \cos^2(\beta/2) \end{bmatrix}$$

It can be seen that a rotation about the x-axis is equivalent to a rotation by $\pi/2$ about z, followed by a rotation about y (since the x axis is now where the y axis was was), and finally a rotation by $-\pi/2$ about z to return the x, y axes to their original positions:

$$e^{-i\alpha I_x} = e^{-i\pi/2 I_z}\, e^{-i\alpha I_y}\, e^{-i\pi/2 I_z}.$$

Hence pulses of duration β along x and y, respectively, are represented by the Wigner rotation matrices

$$D(\pi/2, \beta, -\pi/2) \quad \text{and} \quad D(0, \beta, 0).$$

Acknowledgements

The following people have helped me with this work. It is a pleasure to thank them here.

Dr. Michael R. Morrow, my supervisor, who has been a teacher, colleague and friend throughout my time at Memorial. I have benefitted greatly from his guidance, patience and experimental expertise.

Dr. John de Bruyn and Dr. John Whitehead, members of my supervisory committee, for many helpful discussions and advice. Drs. Kevin Keough and Kaushik Nag of the Biochemistry Department for valuable discussions.

My good friends Romek, Todd, Eugene, Medina, Ken and Rick for support and occasional insanity, and Darius, Ingrid, Gerry and Donna for restoring sanity to acceptable levels.

The secretaries for their help with administration, and all members of the Physics Department for such a pleasant working environment.

The National Science and Engineering Research Council (NSERC) for financial support.